Accepted Manuscript

Numerical simulation of primary break-up and atomization: DNS and modeling study

R. Lebas, T. Menard, P.A. Beau, A. Berlemont, F.X. Demoulin

Please cite this article as: Lebas, R., Menard, T., Beau, P.A., Berlemont, A., Demoulin, F.X., Numerical simulation of primary break-up and atomization: DNS and modeling study, *International Journal of Multiphase Flow International Journal of Multiphase Flow* (2008), doi: 10.1016/j.ijmultiphaseflow.2008.11.005

Numerical simulation of primary break-up and atomization: DNS and modeling study

[Abbreviated title: Numerical Simulation of atomization]

R. Lebas, T. Menard, **P.A. Beau**, **A. Berlemont and F.X. Demoulin**[*]

CNRS CORIA UMR 6614 - University of Rouen
Technopôle du Madrillet - BP 12 - 76801 Saint-Etienne-du-Rouvray Cedex France

ABSTRACT

This work deals with numerical simulations of atomization with high Weber and Reynolds values. A special attention has been devoted to the modelling of primary break-up. Due to progress of direct numerical simulations (DNS) of two-phase flows it is now possible to simulate the primary break-up of a Diesel spray (Menard et al., 2007). The present formulation of the so-called ELSA (Eulerian Lagrangian Spray Atomization model) (Vallet and Borghi, 1999) for atomization is presented and evaluated in the dense zone of the spray by comparison to a DNS based on a coupled Level set/VOF/Ghost fluid method. Once constants and parameters of the model are fixed thanks to comparisons with DNS, the model is tested with experimental data. The liquid and vapour penetrations show a good agreement when they are compared to experiments of Diesel atomization. In particular the influence of the gas temperature is well recovered. For different temperatures, similarly to the experiments, vapour penetrations are unchanged, but the corresponding equivalent ratio fields are strongly modified. Finally, the combustion model ECFM-3Z (Colin and Benkenida, 2004) is joined to the ELSA model and the effect of gas temperature changes on a Diesel spray flame is reproduced.

Keywords: Liquid Atomization, ELSA model, DNS, Primary Breakup

1 Introduction

An important amount of studies have been devoted to the description of the atomization, the main goal is to predict characteristics of the spray as a function of the injection parameters. At the exit of the injector, a very complex flow takes place. It is a two-phase flow, which is composed of liquid and gas, it can be turbulent and surface tension forces play an important role. During the atomization process, the topology of the liquid flow changes drastically from a cylindrical jet to wavy jet, sheets, ligaments, and other not well defined liquid parcels that are usually referred as blobs. Eventually, the liquid becomes a set of droplets: the final spray. Despite

1

the fact that the equations to describe exactly such flows are well known (Ishii, 1975; Kataoka, 1986), their general resolution through the complete process is still a tremendous challenge.

As a consequence, most of the proposed models are based on instability analysis: a basic configuration of the flow at the exit of the injector is considered and the most instable mode is determined. The corresponding wave length is then related to the drop diameter. Many successful descriptions were obtained with these methods, among them the most famous example is the fragmentation of a round liquid jet at low speed, known as the Rayleigh-Plateau instability (Plateau, 1873; Rayleigh, 1878). In many cases, it is not possible to consider that droplets are directly obtained through the first instability. To complete the description, subsequent instabilities have to be considered before droplet generation. For instance, among these models, an elegant description of the atomization was proposed by Marmottant and Villermaux (Marmottant and Villermaux, 2004). It concerns the atomization of a round jet which is surrounded by a high velocity co-flow of gas. The first shear instability produces propagating waves at the surface of the liquid jet. Due to the fluctuating accelerations, a Rayleigh-Taylor instability destabilizes the liquid waves to create ligaments that are finally destroyed through the Rayleigh-Plateau instability (modified due to random stretching) to generate the drops. Depending on the studied cases, other kinds of instabilities may be involved, see (Marmottant and Villermaux, 2004), (Villermaux, 2007) and references therein.

Taking as an example the atomization of cylindrical jet, most of the practical modelling approaches are still based on linear instabilities. The successful applications of Reitz's models (Reitz, 1987; Beale and Reitz, 1999) demonstrate how useful is this kind of approach. Nevertheless, it can be interesting to overtake linear analysis restrictions to compute actually what happens in the flow up to the final spray. To overcome these limitations, Yi and Reitz (Yi and Reitz, 2002; Yi and Reitz, 2004) propose an approach where the break-up characteristics of the jet are calculated by tracking the wave growth on the surface of each liquid blob using a one-dimensional Eulerian approach. To go further, an axisymmetric boundary element method is

2

used to simulate the primary atomization, (Yoon and Heister, 2004; Park et al., 2005; Yoon, 2005). Due to symmetry, ring ligaments are produced. To successfully recover droplet distributions, the characteristics of the droplets that are issued from the ring ligaments are obtained through linear instability analysis (Ponstein, 1959).

In the present work, we would like to come back to the initial problem that is to solve completely the nonlinear two phase flow equations. Indeed, for many industrial devices, the atomization process is a key parameter, for instance in Diesel injection. In such applications, the injection takes place at high Weber and Reynolds numbers. It is necessary to reach the expected fuel load with an injection period of the order of one millisecond. The injection has to be fast and the induced processes like vaporization and mixing have also to be very efficient and quick. To obtain an appropriate spray, the geometry of the injector itself is optimized together with the injection conditions (up to 2000 bar for the injection pressure). With such conditions, the global flow in the combustion chamber (in particular air entrainment) is controlled by the injection itself. To represent such flows, we need a suitable representation of the atomization that gives us not only the size distribution (when it is possible to define it) but the velocity field that depends strongly on the density field. This shows the importance to design models that are able to represent the liquid phase dispersion accurately. Thus, in addition to droplet size distribution, it is necessary to predict the two phase flow behaviour from the injector tip and to be able to account for any boundary condition at the exit of the injector. Notice that much more theoretical and experimental studies are devoted to the determination of the size distribution than to the determination of the liquid volume fraction field. Indeed the determination of the liquid volume fraction is often difficult, but in complement of the size distribution it is certainly interesting to know to which amount of liquid the size distribution corresponds. To be able to account for the geometry of the injector and to represent the flow in the engine, a complete nonlinear simulation of the flow has to be achieved.

The major difficulties arise in the so-called primary break up that is the first step of the atomization. It takes place in a zone where the spray is very dense. In this area the liquid volume fraction is close to one and the liquid surface topology is very complex. As a consequence, it is very difficult to get experimental results in order to characterize this zone. Some of the experiments that are realized for this kind of atomization processes are based on methods that are known to give well established results for dilute spray. For instance there is the PDA (Phase Doppler Analyzer), the particle size analyzers based on laser diffraction, the Mie scattering technique to measure liquid penetration. However, the domain of application of such methods is rejected far downstream from the region where the primary break up takes place. Most of these methods are designed to measure the characteristics of liquid droplets, but they failed in the primary break up part of the jet. Few methods are dedicated to the dense part of the spray, among them there are the LCV (Laser Correlation Velocimetry) technique (Chaves et al., 2004), X-ray measurements (Yue et al., 2001; Cai et al., 2003), ballistic imaging (Linne et al., 2006) and other methods based on image processing (Blaisot and Yon, 2005). Despite these new insights, physical mechanisms controlling the dense part of the spray are not yet completely elucidated and complete data set describing this zone does not exist. To improve the knowledge of break up processes, a promising tool is the direct numerical simulation (DNS). It can be used to create a numerical experiment for region where no experimental data can be obtained. Notice that this numerical approach has the drawback to be limited to very small domains. But, the primary break up takes place in a quite small area which is often limited by few injector diameters in the downstream direction. Therefore it is actually very appealing to test such a method even with its inherent limitations in order to complete our knowledge.

Direct numerical simulations of interface tracking have been recently proposed by Menard et al. (Menard et al., 2007) and they are used here to obtain data in order to build and to validate a

4

second approach, which is based on an average description of the two phase flow that is of practical interest to simulate Diesel combustion.

In the first part of this paper, the underlying numerical methods used for the DNS and the characteristics of a simplified test case close to Diesel injection conditions are described. In the second part the Eulerian Lagrangian Spray Atomization (ELSA) model (Vallet and Borghi, 1999; Vallet et al., 2001) is presented. A special attention is devoted to describe realistically the primary break up. This complete model was already tested but against experimental data far from the injector (Blokkeel et al., 2003; Lebas et al., 2005; Beheshti et al., 2007). Here, it is tested for the first time by comparisons with data in the primary break-up zone of the jet thanks to the DNS results. In particular, quantitative comparisons for the liquid volume fraction and the liquid surface density are obtained. The aim of the third part is to demonstrate the ability of the ELSA model to handle a complete case from atomization to combustion. Several comparisons with experiments are reported to show the relevance of this approach.

2 Direct Numerical Simulation of the primary break up

In the primary break-up of a jet, the gas/liquid interface presents several different behaviours under interface pinching or merging. Moreover, liquid parcels are generated by liquid detachments from the liquid core and they are highly influenced by coalescence or secondary break-up. Thus, the numerical method must describe the interface motion precisely consequently Ménard et al. (Menard et al., 2007) chose to develop a 3D code which is based on the level set method. The ghost fluid method (Fedkiw et al., 1999) is used to take into account sharp discontinuities at the interface in order to avoid artificial smoothing of the interface. One drawback of the level set method is to not be mass conservative when the discretization is not enough refined. Thus the level set method has been coupled with the VOF method to ensure

mass conservation (Sussman and Puckett, 2000). A projection method is used to solve incompressible Navier–Stokes equations. Specific care has been devoted to improving simulation capabilities with MPI parallelization.

We briefly recall the level set method, the coupling between the level set and VOF techniques and the ghost fluid method that are extensively described in previous work (Menard et al., 2007). Then the numerical test case to explore the primary break-up is presented.

2.1   Numerical techniques, Interface tracking, Coupling VOF and Level Set methods

Level set methods (LS) are based on the use of a continuous function ϕ to describe the interface (Sethian, 1996; Osher and Fedkiw, 2001). That function is defined as the signed distance between any points of the domain and the interface, thus the 0 level curve provides the interface location. The motion of the interface in a given velocity field V reads:

$$\frac{\partial \phi}{\partial t} + \mathbf{V}.\nabla \phi = 0 \tag{1}$$

To avoid singularities in the distance function field, the 5th-order WENO scheme for convective terms is used. The unit normal vector and the curvature of the interface can be easily evaluated with the level set function by:

$$\mathbf{n} = \frac{\nabla \phi}{|\nabla \phi|} \qquad \kappa(\phi) = \nabla \cdot \mathbf{n} \tag{2}$$

When the level set method is carried out, high velocity gradients can produce wide spreading and stretching of the level set, and ϕ will no longer remain a distance function. A redistancing algorithm (Sussman et al., 1998) is thus applied to keep ϕ as the signed distance to the interface.

Numerical computations of Eq. (1) and the redistance algorithm can induce mass loss in under-resolved regions. This is the main drawback of level set methods. To improve mass conservation, extensions of the method can be developed (Sussman and Puckett, 2000; Enright et al., 2002; Olsson and Kreiss, 2005; van der Pijl et al., 2005). Specific studies have been

6

developed to evaluate some of these methods (Menard et al., 2007), and we observed that the CLSVOF (Sussman and Puckett, 2000) is well adapted to capture atomization process.

The main idea of this method is to benefit from the advantage of each strategy: to minimize the mass loss through the VOF and to keep a fine description of interface properties with the level set. Details of the level set and VOF methods coupling have been previously described (Sussman and Puckett, 2000), and with some improvements to capture fine ligaments (Menard et al., 2007).

The Level Set method is coupled with a projection method for the direct numerical simulation of incompressible Navier-Stokes equations, where the density and the viscosity depend on the sign of the Level Set function. To finalize the description of the two phase flow, jump conditions across the interface are taken into account with the Ghost Fluid (GF) method.

In the GF method, ghost cells are defined on each side of the interface   (Kang et al., 2000; Liu et al., 2000) and appropriate schemes are applied for variable jumps. As defined above, the interface is characterized through the distance function, and jump conditions are extrapolated on some nodes on each side of the interface. Following the jump conditions, the discontinued functions are extended continuously and then derivatives are estimated. More details on implementing the Ghost Fluid Method to solve the Poisson equation with discontinuous coefficients can be found elsewhere (Liu et al., 2000).

2.2   A numerical configuration to explore primary break-up

The above described DNS code based on a coupled method ``Level Set - Volume Of Fluid - Ghost fluid'' is used to get an insight of the dense zone of the spray. It is particularly interesting because it completes the available experimental data in a region of interest which is still difficult to reach with existing experimental techniques.

7

The numerical conditions are presented in Table 1. The aim is to simulate an injection that is representative of Diesel injection. The diameter of the injector nozzle has been chosen equal to $100\mu m$ and the surface tension is equal to $0.06 kg.s.^{-2}$. The gas in the computational domain is initially at rest.

Table1 (about here)

The surface tension has been overestimated in order to limit the minimum size of droplets. It is assumed that no secondary break up occurs for the smallest droplet. This implies that the Weber number is at least smaller than 10 and gives a minimum droplet diameter equal to 2.4μm when the surface tension is 0.06 (rather than 0.02 in Diesel injection). Nevertheless, it is still possible that such a spray generates very small liquid inclusions. For instance, following a collision it is possible to create satellite droplets that are very small. Below a certain characteristic size, which is related to the mesh size, the DNS code does not describe properly the physics of the flow. For instance this can induce numerical rupture of ligaments, numerical break-up of liquid sheets or in the worst case disappearance of the smallest droplets. For this latter case, a huge improvement has been obtained by using the VOF method in combination with the Level-Set approach: the loss of mass is negligible in the presented test case. These numerical limitations have to be kept in mind when discussing the results. It is worth noting that the present conditions are not completely representative of Diesel injections that are currently used in industry. Nevertheless, this application belongs to the category of injection with high values of Weber and Reynolds numbers.

The total size of the calculation domain is $0.3mm \times 0.3mm \times 2.2mm$. The uniform 3D Cartesian grid size is 128×128× 896, and the grid spacing is 2.36μm. At injection, the Reynolds number $U_{liq}D/\nu_{liq}$ in the liquid is equal to 5800. Extensive results on the primary break-up of the jet are provided in Ménard et al (2007).

To illustrate the ability of the Level Set/VOF/Ghost Fluid method to simulate the primary atomization zone of a turbulent liquid jet, Fig. 1 shows the spray which is issued from the nozzle after the initialization period. The interface is given by the 0 level of the level set and a numerical algorithm has been set up to extract all the different liquid parcels. The top figure shows the whole spray. The middle figure represents only the liquid part of the spray that is attached to the tip of the injector. Finally the bottom figure represents all the other liquid blobs. It is very clear that for this kind of injection, after roughly 20 diameters, the spray is not fully atomized. The most important part of the liquid is still attached to the injector in a more or less continuous flow. This simulation confirmed that a representation of such a spray as a set of isolated spherical droplets is not realistic. This gives information for modelling and also for experiments. Indeed, what would be the measurement result of such sprays using a phase Doppler anemometer (PDA)? Probably, only small droplets that are detached from the spray would give validated measurements. Consequently, a very biased estimation of the mean diameter would be obtained. Considering only the detached part of the spray, it is possible to observe that some spherical droplets exist but many other liquid parcels take different shapes. These computations highlight the necessity to define this spray with a more general parameter than a mean diameter. In the following, some attempts in that direction are carried out by using instead of the diameter, the mean surface density.

Fig. 1: (about here)

3 ELSA model for atomization, description of the primary break-up

3.1   Overview of the Eulerian Lagrangian spray atomization model: basic equations

9

The Eulerian Lagrangian Spray Atomization (ELSA) model was designed originally to describe atomization of flows with high Weber and Reynolds values (Vallet and Borghi, 1999; Vallet et al., 2001). In the ELSA model, the two phase flow is studied as a single phase flow composed of two species, liquid and gas, with highly variable density.

It is possible to use multiphase flow formalism in combination with the ELSA model. Nevertheless in Diesel injections it is not straightforward to define a discrete phase and a carrier phase as it is commonly requested by multiphase flow approaches. Indeed, just at the exit of the injector nozzle, the proportion of the liquid phase is very high and this phase is certainly not composed of discrete particles. Moreover, bubbles could be present in the liquid flow due to penetration of the surrounding gas during the break-up process and to previous cavitation inside the nozzle injector. In this case, the carrier phase would be the liquid and the discrete phase the gas bubbles. Of course, further downstream, a spray is created where the carrier phase is the gas and the discrete phase corresponds to liquid droplets. Between these two limits, a two phase flow exists with unclear discrete and carrier phases. In the ELSA model the single phase approach allows the choice of both carrier and discrete phases to be avoided. It is worth noting that some choices are still required in the closure of the different submodels. In the limit of infinite Weber values, there is a certain similarity between turbulent gas mixing and the complex phenomena occurring in the primary break-up zone. Hence, we believe that this transition zone can be more easily handled with the single phase flow formalism of the ELSA model because it is similar to the formalism used for the turbulent mixing of two gases with different densities.

Since we consider flows with high Reynolds values, the turbulence has to be taken into account. The accuracy of different RANS turbulence models when they are applied to turbulent two phase flows was studied previously (Demoulin et al., 2007). It was shown that the standard k-ε turbulence model (Launder and Spalding, 1974) is able to reproduce the main characteristics of the two-phase flow if special care is devoted to the modelling of the turbulent mass flux. The transport equation for the mean mixture velocity is written, neglecting terms that

are related to the surface tension and the laminar viscosity in accordance to the hypothesis of high Weber and Reynolds values reads:

$$\frac{\partial \overline{\rho}\tilde{u}_i}{\partial t} + \frac{\partial \overline{\rho}\tilde{u}_j\tilde{u}_i}{\partial x_j} = -\frac{\partial R_{ij}}{\partial x_j} - \frac{\partial \overline{p}}{\partial x_i} \tag{3}$$

Considering a variable φ, its Reynolds average is noted $\overline{\varphi}$ and the corresponding fluctuation is noted φ'. The mass weighted Favre average is $\tilde{\varphi} = \overline{\rho\varphi}/\overline{\rho}$ and the corresponding fluctuation is noted φ''. Thus, $\overline{\rho}$ represents the mean mixture density, $\tilde{u}$ is the Favre averaged mixture velocity and $\overline{p}$ is the mean pressure. The k-ε equations are written in their standard single flow formalism without modification:

$$\frac{\partial \overline{\rho}\tilde{k}}{\partial t} + \frac{\partial \overline{\rho}\tilde{u}_j\tilde{k}}{\partial x_j} = \frac{\partial}{\partial x_j}\left(\overline{\rho}\frac{v_t}{\mathrm{Pr}_k}\frac{\partial \tilde{k}}{\partial x_j}\right) - \overline{\rho}R_{ij}\frac{\partial \tilde{u}_j}{\partial x_i} - \overline{u_j''}\frac{\partial \overline{p}}{\partial x_j} - \overline{\rho}\tilde{\varepsilon}, \tag{4}$$

$$\frac{\partial \overline{\rho}\tilde{\varepsilon}}{\partial t} + \frac{\partial \overline{\rho}\tilde{u}_j\tilde{\varepsilon}}{\partial x_j} = \frac{\partial}{\partial x_j}\left(\overline{\rho}\frac{v_t}{\mathrm{Pr}_\varepsilon}\frac{\partial \tilde{\varepsilon}}{\partial x_j}\right) + C_{\varepsilon_1}\frac{\tilde{\varepsilon}}{\tilde{k}}\left(-\overline{\rho}R_{ij}\frac{\partial \tilde{u}_j}{\partial x_i} - \overline{u_j''}\frac{\partial \overline{p}}{\partial x_j}\right) - C_{\varepsilon_2}\overline{\rho}\frac{\tilde{\varepsilon}^2}{\tilde{k}} \tag{5}$$

Together with these equations, the Boussinesq relation is used to close the Reynolds stress tensor:

$$v_t = C_\mu\frac{\tilde{k}^2}{\tilde{\varepsilon}} \quad \text{and} \quad R_{ij} = \overline{\rho u_i''u_j''} = -\mu_t\left(\frac{\partial \tilde{u}_i}{\partial x_j} + \frac{\partial \tilde{u}_j}{\partial x_i} - \frac{2}{3}\frac{\partial \tilde{u}_k}{\partial x_k}\delta_{ij}\right) + \frac{2}{3}\overline{\rho}\tilde{k}\delta_{ij}. \tag{6}$$

Finally, the Reynolds average of the Favre fluctuation of the velocity $\overline{u_i''}$ is exactly related to the turbulent liquid mass flux R_{iY_l} through:

$$\overline{u_i''} = \overline{\rho}\left(1/\rho_l - 1/\rho_g\right)R_{iY_l}, \tag{7}$$

where $R_{iY_l} = \overline{\rho u_i''Y_l''}/\overline{\rho}$ and Y_l is the liquid mass fraction. It is expected that the application of the k-ε model for two phase flows requires some modifications. For instance, in multiphase flow formalisms it is proposed to consider one equation for the turbulent kinetic energy of the carrier phase and one for the discrete phase. It is even possible to consider a cross correlation term: the velocity fluctuation of the carrier phase correlated to the velocity fluctuation of the

discrete phase (Simonin, 2000). Here, the standard model is kept with only one kinetic equation to represent the total kinetic energy of the mixture. This is certainly a strong simplification, it would be interesting to develop and test additional equations to represent the repartition of the turbulent kinetic energy in each phase. Such equations which are validated in the dense part of the spray are not yet available in multiphase approaches.

Since the liquid and gas phases are considered as species in this single flow approach, the corresponding transport equation is very important. Indeed the liquid dispersion is entirely represented through the following equation:

$$\frac{\partial \overline{\rho}\widetilde{Y}_l}{\partial t} + \frac{\partial \overline{\rho}\widetilde{Y}_l\widetilde{u}_j}{\partial x_j} = -\frac{\partial \overline{\rho Y_l u_j''}}{\partial x_j} - \overline{\rho}\dot{m}_{v,ELSA}\widetilde{\Omega} = -\frac{\partial \overline{\rho}R_{jY_l}}{\partial x_j} - \overline{\rho}\dot{m}_{v,ELSA}\widetilde{\Omega} \ . \tag{8}$$

The second term of the RHS concerns the vaporization; it will be discussed in the next section. This equation contains only one unclosed term, namely the turbulent liquid flux R_{jY_l}. For turbulent single phase flows, the gradient closure approximation is generally applied:

$$R_{jY_l} = -\frac{v_t}{Sc_t}\frac{\partial \widetilde{Y}}{\partial x_i}. \tag{9}$$

Nevertheless, because the phases are strictly separated, it is possible to derive the exact following relation (Demoulin et al., 2007):

$$R_{jY_l} = \widetilde{Y}_l\left(1 - \widetilde{Y}_l\right)\!\left(\overline{u}_j\big|_l - \overline{u}_j\big|_g\right) = \widetilde{Y}_l\left(\overline{u}_j\big|_l - \widetilde{u}_j\right). \tag{10}$$

This relation shows the strong link between the turbulent liquid flux and the difference of velocities between the mean liquid velocity $\overline{u}_j\big|_l$ and the mean gas velocity $\overline{u}_j\big|_g$. If the density ratio between phases is close to one, then the inertial effect vanishes. Thus, the slip velocity between phases becomes zero. But a non zero phase velocity difference ($\overline{u}_j\big|_l - \overline{u}_j\big|_g$) is still possible if the phase concentrations are not uniform in space. Indeed, this limit corresponds to gas mixing where the gradient closure Eq. (9) can be applied faithfully. Additionally, the relation

12

Eq. (10) shows that even with this single flow approach it is possible to recover the different phase velocities. For instance, knowing the mean mixture velocity thanks to its transport equation Eq. (3), the mean liquid velocity is easily obtained as a function of the turbulent liquid flux:

$$\bar{u}_j\Big|_l = \frac{R_{jY_l}}{\tilde{Y}_l} + \tilde{u}_j .$$

This is the basis of the drift flux model (Ishii, 1977; Ishii and Ibiki, 2006), but in this case algebraic relations are provided to close the turbulent mass flux R_{jY_l}. By adapting second order models for turbulent mixing, it is possible to develop three equations for the three turbulent fluxes R_{jY_l}. The resulting model is clearly equivalent to multiphase flow approaches. This is the so-called quasi-multiphase model (Beau et al., 2005).

In order to complete these equations, the mean density is given by:

$$\frac{1}{\bar{\rho}} = \frac{\tilde{Y}_l}{\rho_l} + \frac{1-\tilde{Y}_l}{\rho_g} \tag{11}$$

The dispersion of the liquid is entirely described by the previous equations but the complete model incorporates an additional equation for the liquid-gas surface density.

3.2 A more general notion than the droplet diameter: the mean liquid/gas interface density $\tilde{\Omega}$

The ELSA model is an atomization model. It is thus expected to predict the characteristics of the liquid droplets or blobs in the dense part of the spray such as velocities or sizes. Based on DNS results it is clear that the liquid phase cannot be represented as a set of droplets during the primary break-up. Moreover this dense zone extends far downstream from the injector (more than 20 diameters in our case). Considering the DNS results in Fig. 1, it would be surprising that models assuming spherical droplets, incorporating drag coefficient for isolated solid spheres, give accurate results in this case. Indeed, the determination of the relevant physical variables that

13

can be used to characterize such a liquid surface is still an open problem. At least the most important variable is certainly the quantity of liquid interface. The local surface density can be defined in term of generalized function and an exact equation can be derived for such a quantity (Morel, 2007). Despite this theoretical work, the general form of this equation once filtered or averaged has to be closed. The first equation for the mean liquid surface density was proposed in (Vallet and Borghi, 1999; Vallet et al., 2001). This equation was postulated by analogy with the transport equation of the flame surface density of Marble and Broadwell (Marble and Broadwell, 1977). In our point of view, the first interest of this equation is to avoid any assumption concerning the shape of the liquid surface and to try to describe realistically this two phase flow. Later, a surface density equation was used in a multiphase Eulerian model of atomization in order to avoid the problem of mesh dependency occurring with Lagrangian method (Iyer and Abraham, 2003).

The precise definition of the liquid/gas interface density $\overline{\Sigma}$ (m^{-1}) is the quantity of liquid/gas interface per unit of volume. In this paper, we rather use the quantity of liquid/gas interface per unit of mass $\tilde{\Omega} = \overline{\Sigma}/\overline{\rho}$ ($m^2.kg^{-1}$) to simplify the equation and more especially the treatment of the diffusive term. A possible formulation for this equation is:

$$\frac{\partial \overline{\rho}\tilde{\Omega}}{\partial t} + \frac{\partial \overline{\rho}\tilde{\Omega}\tilde{u}_j}{\partial x_j} = \frac{\partial}{\partial x_j}(\overline{\rho}\tilde{\Omega}(\tilde{u}_j - \overline{u}_j\big|_\Omega))$$
$$+ \overline{\rho}(\dot{\tilde{\Omega}}_{mixture} + \dot{\tilde{\Omega}}_{stress} + \dot{\tilde{\Omega}}_{breakup} + \dot{\tilde{\Omega}}_{coalesence} + \dot{\tilde{\Omega}}_{vaporization}) \quad (12)$$

The first term of the RHS is unclosed since it contains $\overline{u}_j\big|_\Omega$ which is the mean surface velocity. This quantity is generally unknown excepted in dilute cases where droplets (respectively bubbles) can be defined. Moreover, if all droplets (respectively bubbles) have the same size then $\overline{u}_j\big|_\Omega = \overline{u}_j\big|_l$ (respectively $\overline{u}_j\big|_\Omega = \overline{u}_j\big|_g$). These conditions are very restrictive. We believe that it is better for atomization process approaches to model the first term of the RHS as a turbulent diffusive term for the surface density. The other terms of the RHS correspond to:

- $\overline{\rho}\dot{\tilde{\Omega}}_{mixture}$: production by turbulent mixing between liquid and gas

14

- $\overline{\rho}\dot{\tilde{\Omega}}_{stress}$: production by the mean shear stress

- $\overline{\rho}\dot{\tilde{\Omega}}_{breakup}$: production by break-up

- $\overline{\rho}\dot{\tilde{\Omega}}_{coalesence}$: production/destruction by coalescence

- $\overline{\rho}\dot{\tilde{\Omega}}_{vaporization}$: production/destruction by vaporization

These terms have to be precisely closed. Until now, there are no firmly established models which are able to represent the surface density evolution in all the possible cases. The most direct method to close the surface density equation concerns the case where the spray is composed of spherical droplets. Assuming that the equation for the diameter distribution is known (using classical models for break-up, collision and vaporization) an equation for the surface density is recovered by integrating the second moment of this distribution (Kocamustafaogullari and Ishii, 1995; Ishii and Ibiki, 2006). If additionally it is assumed that all droplet diameters are identical, the diameter distribution is completely known from the liquid volume fraction and the surface density. Nevertheless this approach does not stand in the vicinity of the injector where the droplets are not yet formed. Since the first proposition (Vallet and Borghi, 1999; Vallet et al., 2001) for new source terms inspired from turbulent combustion framework, several evolutions have taken place (Iyer et al., 2002; Blokkeel et al., 2003; Lebas et al., 2005; Beau et al., 2006; Jay et al., 2006; Beheshti et al., 2007; Sidhu and Burluka, 2008). Based on the previously cited literature and our practice, a possible transport equation for $\tilde{\Omega}$ is given here:

$$\frac{\partial \overline{\rho}\tilde{\Omega}}{\partial t} + \frac{\partial \overline{\rho}\tilde{\Omega}\tilde{u}_j}{\partial x_j} = \frac{\partial}{\partial x_j}(\overline{\rho}\frac{\nu_t}{Sc_{t\Omega}}\frac{\partial}{\partial x_j}\tilde{\Omega}) + \Psi(S_{init} + S_{turb}) \\ + (1-\Psi)(S_{coll} + S_{2ndBU}) + S_{vapo} \tag{13}$$

On the RHS of the equation Eq. (13), the first term represents the turbulent flux of interface. It is closed using a turbulent diffusion term. As discussed above for the liquid turbulent flux (Eq. (8)), this approach is valid if there is no mean slip velocity between the liquid and the gas, but if a phase velocity difference still exists. This is the case for very small liquid particles with no

15

inertia. This can be also the case in the very dense part of the spray, where the amount of liquid is so important that motion of gas fluid particles is controlled by the liquid motion. If there are any reasons to assume that the slip velocity between phases can be important, this model would have to be improved. Here, the turbulent Schmidt number dedicated to the turbulent flux of the surface density is taken equal to the one used for the liquid mass fraction ($Sc_t = Sc_{t\Omega}$).

As discussed above, source terms of the surface density equation can be obtained from two different approaches: a first one for the dense part of the spray where no droplets can be defined and a second one far away from the injector where droplets are already formed. To link continuously both approaches through the whole spray, a repartition function Ψ is introduced. It is used as an indicator of the dense or dilute region in the spray. In this work, Ψ is chosen in order to return a value of 1 in the dense region and a value of 0 in the dilute region. The transition between these two cases is made via a linear regression, as it can be seen in Fig. 2.

Fig. 2: (about here)

ϕ_{dense} and ϕ_{dilute} correspond to specific values of the liquid volume fraction ϕ_l. They are obtained thanks to the following relation:

$$\phi_l = \frac{\overline{\rho}\widetilde{Y}_l}{\rho_l} \tag{14}$$

They can be considered as numerical parameters, but during all this study they have been fixed to: $\phi_{dense} = 0.5$ and $\phi_{dilute} = 0.1$. Otherwise, each source term S_i of the equation Eq. (13) models a phenomenon that can be encountered by the liquid blobs or droplets.

S_{init} can be considered as an initialization term, taking high values near the injector nozzle, where mass fraction gradients take their highest values. It corresponds to the minimum production of liquid-gas interface density induced by liquid-gas mixing (Beau et al., 2006).

$$S_{init} = \frac{12\overline{\rho}\mu_t}{\rho_l \rho_g Sc_t l_t} \frac{\partial \widetilde{Y_l}}{\partial x_i} \frac{\partial \widetilde{Y_l}}{\partial x_i}. \tag{15}$$

This term is derived to obtain surface density greater than a minimum surface density defined by:

$$\Sigma_{min} = \frac{\phi_l (1 - \phi_l)}{l_t}. \tag{16}$$

This expression of Σ_{min} represents the probability to have both liquid and gas divided by a characteristic scale. First wrinkles of the surface are supposed to have a characteristic size equal to the integral turbulent length scale. This formulation is not firmly established yet and has to be studied in the future. Nevertheless we checked that this source term is important only in the vicinity of the injector. Once initial surface density is created, this source term becomes negligible by comparison with the other source terms. In that sense it can be seen as a model to initiate automatically the surface density equation as soon as liquid-gas mixing occurs.

S_{turb} corresponds to the production/destruction of liquid-gas interface density due to the turbulent flow stretching and the effects of collision and coalescence in the dense part of the spray. It is assumed to be driven by a turbulent time scale τ_t. This production/destruction term is defined in order to reach an equilibrium value of the surface density Ω_{den}^*. It corresponds to the quantity of surface that would be obtained by keeping constant the total mixture turbulent kinetic energy and the liquid volume fraction. This surface density can be expressed in term of a Weber number defined as the ratio between the total kinetic energy per unit of volume and the total surface energy per unit of liquid volume We_{den}^*:

$$We_{den}^* = \frac{\overline{\phi_l}\widetilde{k}}{\sigma_l \Omega_{den}^*}, \tag{17}$$

σ_l corresponds to the surface tension of the liquid phase. The equilibrium value of this Weber number is unknown at our best knowledge especially for liquid-gas flows with high values of liquid volume fraction. It is then assumed that the total energy is equally distributed between the

17

kinetic energy and the surface energy. Accordingly to determine Ω^*_{den}, the value of We^*_{den} is set to 1.0 in this paper. The modelling of We^*_{den} is thus a first step that requires further work to be definitely established. The final expression of the source term is:

$$S_{turb} = \frac{\overline{\rho}\widetilde{\Omega}}{\tau_t}\left(1 - \frac{\widetilde{\Omega}}{\Omega^*_{den}}\right), \quad \Omega^*_{den} = \frac{\overline{\phi}_l\widetilde{k}}{\sigma_l We^*_{den}} \text{ and } We^*_{den} = 1 \ . \tag{18}$$

Concerning the dilute part of the spray, the aim is to derive the classical model used for dilute spray in term of surface density, for instance in a Lagrangian framework. That requires to define an equivalent diameter. The Sauter mean diameter is obtained thanks to the liquid-gas interface density and the mean liquid mass fraction:

$$D_{32} = \frac{6\widetilde{Y}_l}{\rho_l\widetilde{\Omega}}. \tag{19}$$

Additionally, to avoid the repartition of source terms through the function Ψ, it would be interesting that both dense and dilute source terms converge to the same formulation in the transition zone. This is partly possible with the collision-coalescence source term:

$$S_{coll} = \frac{\overline{\rho}\widetilde{\Omega}}{\tau_{coll}}\left(1 - \frac{\widetilde{\Omega}}{\Omega^*_{coll}}\right), \tag{20}$$

This source term is driven by a collision time scale τ_{coll}. Several models have been proposed to represent the collision effect on the evolution of the surface density (Vallet and Borghi, 1999; Vallet et al., 2001; Iyer et al., 2002; Iyer and Abraham, 2003). Here, based on the particle collision theory, the model for τ_{coll} is:

$$\tau_{coll} = \frac{L_{coll}^3}{S_{eff}\Delta V_{coll}}, \tag{21}$$

L_{coll} is the mean free path, S_{eff} is the cross section of collision and ΔV_{coll} is the characteristic velocity of collision. These variables have to be estimated through available model variables. The following approximations have been done:

18

$$L_{coll} \approx N_d^{-1/3} = \frac{\rho_l^2 \overline{\rho} \widetilde{\Omega}^3 L_{coll}^3}{36\pi \widetilde{Y}_l^2} \ , \ S_{eff} \approx \frac{36\pi \widetilde{Y}_l^2 \rho_l^2 \overline{\rho} \widetilde{\Omega}^3}{\rho_l^2 \overline{\rho} \widetilde{\Omega}^2} \text{ and } \Delta V_{coll} \approx \sqrt{\frac{2}{3}\widetilde{k}} . \quad (22)$$

Finally the collision time scale is estimated by:

$$\tau_{coll} \approx \frac{1}{\overline{\rho}\widetilde{\Omega}\sqrt{\frac{2}{3}\widetilde{k}}} \quad (23)$$

Based on this time scale, the collision source term induces an equilibrium value Ω_{coll}^* of the surface density that has to be determined. The relevant Weber number to characterize the collision between two droplets is classically defined by:

$$We_{coll} = \frac{\rho_l \ \Delta V_{coll}^2 \ D}{\sigma_l} \approx \frac{4\widetilde{Y}_l \widetilde{k}}{\sigma_l \widetilde{\Omega}} , \quad (24)$$

where D is the droplet diameter. It is expressed in term of the surface density Ω thanks to Eq. (19). The previous approximation for the collision velocity (Eq. (22)) is used. Based on the work of Qian and Law (Qian and Law, 1997), the value of We_{coll} that separates break-up and coalescence regime is estimated as $We_{coll}^N = 12$. This value is not directly the equilibrium Weber number that we are looking for. Indeed, the kinetic energy and the surface energy change during the collision process in the whole spray. Assuming a conservation of the total energy (kinetic and surface energy) during the collision process, the following relation has been proposed (Beau et al., 2006) to find the final equilibrium diameter D_{32}^* :

$$D_{32}^* = D_{32} \frac{1 + \dfrac{We_{coll}^N}{6}}{1 + \dfrac{We_{coll}}{6}} , \quad (25)$$

Finally the equilibrium Weber number is given by:

$$We_{coll}^* = \frac{\rho_l \ \dfrac{2}{3}\widetilde{k} \ D_{32}^*}{\sigma_l} , \quad (26)$$

19

In addition, any relevant models that are used for dispersed sprays would be adapted to improve the surface density equation. The source term S_{2ndBU} deals with the production of liquid-gas interface density due to the effects of secondary break-up in the dilute spray region. This source term comes from the model first proposed by Pilch and Erdman (Pilch and Erdman, 1987):

$$S_{2ndBU} = Max\left[\frac{\overline{\rho}\tilde{\Omega}}{\tau_{2ndBU}} \left(1 - \frac{\tilde{\Omega}}{\tilde{\Omega}^*_{2ndBU}} \right), 0 \right].$$ (27)

The break-up process increases the surface density. For that reason only positive values of this source term are taken into account. The Weber number associated to this process is based on the gas density ρ_g, on the liquid-gas relative velocity Δv_{rel} and on the droplet diameter:

$$We_{2ndBU} = \frac{\rho_g \Delta v_{rel}^2 D}{\sigma_l} \approx \frac{6\rho_g \Delta v_{rel}^2 \tilde{Y}_l}{\rho_l \sigma_l \tilde{\Omega}}.$$ (28)

The main problem concerns the approximation of Δv_{rel}, in the present study this velocity is approximated by the mean relative phase velocity $\overline{u}_j\big|_l - \overline{u}_j\big|_g$. Accordingly, thanks to Eq. (10) the model for the turbulent liquid flux has to be used to determine Δv_{rel}. The estimation of the break-up time scale τ_{2ndBU} is (Pilch and Erdman, 1987):

$$\tau_{2ndBU} = T \frac{D_{32}}{\Delta v_{rel}} \sqrt{\frac{\rho_l}{\rho_g}}.$$ (29)

The parameter T is given as a function of the Weber number We_{2ndBU} (Pilch and Erdman, 1987). The break-up process occurs until an equilibrium value of the Weber number We^*_{2ndBU} is reached. It corresponds to an equilibrium value of surface density Ω^*_{2ndBU} that is obtained thanks to Eq. (28). The equilibrium Weber number is given by:

$$We^*_{2ndBU} = 12(1 + 1.077Oh^{1.6}).$$ (30)

20

where Oh is the Ohnesorge number. In the following application, the liquid viscosity is relatively small and leads to a small Ohnesorge number: $We^*_{2ndBU} \approx 12$.

Finally the modelled transport equation for the surface density $\tilde{\Omega}$ is:

$$\frac{\partial \overline{\rho}\tilde{\Omega}}{\partial t} + \frac{\partial \overline{\rho}\tilde{\Omega}\tilde{u}_j}{\partial x_j} = \frac{\partial}{\partial x_j}(\overline{\rho}\frac{v_t}{Sc_{t\Omega}}\frac{\partial}{\partial x_j}\tilde{\Omega}) + \Psi\left(\alpha_1 \frac{12\overline{\rho}\mu_t}{\rho_l\rho_g Sc_t l_t}\frac{\partial \tilde{Y}_l}{\partial x_i}\frac{\partial \tilde{Y}_l}{\partial x_i}. + \alpha_2 \frac{\overline{\rho}\tilde{\Omega}}{\tau_t}\left(1 - \frac{\tilde{\Omega}}{\Omega^*_{den}}\right)\right)$$
$$+ (1-\Psi)(\alpha_3 \frac{\overline{\rho}\tilde{\Omega}}{\tau_{coll}}\left(1 - \frac{\tilde{\Omega}}{\Omega^*_{coll}}\right) + \alpha_4 Max\left[\frac{\overline{\rho}\tilde{\Omega}}{\tau_{2ndBU}}\left(1 - \frac{\tilde{\Omega}}{\tilde{\Omega}^*_{2ndBU}}\right),0\right]) \quad . \quad (31)$$

The numerical parameters are the following: $\alpha_1 = \alpha_2 = \alpha_3 = \alpha_4 = 1$, the turbulent Schmidt numbers $Sc_{t\Omega} = Sc_t = 1$ and the Weber numbers used to determine $\Omega^*_{den} = f_{dens}\left(W^*_{dens} = 1\right)$, $\Omega^*_{coll} = f_{coll}\left(W^N_{coll} = 12\right)$, $\Omega^*_{2ndBU} = f_{2ndBU}\left(W^*_{2ndBU} \approx 12\right)$.

4 Validation and application of the ELSA model

4.1 Comparisons between DNS and ELSA calculations

The DNS test case presented previously is used now to validate the ELSA model in the dense zone of the spray. The characteristics of the test case are identical to those that are presented in Table 1. The computational domain used for ELSA calculations is a cylinder with a diameter of 2mm and a high of 5mm. It recovers completely the computational domain used for the DNS (see section 2.2). For the ELSA calculations, two different mesh refinements have been tested. First grid M1 contained 70000 cells, and 140000 cells are used in the second grid M2. Boundaries conditions are similar for DNS and ELSA computation: there are free boundary conditions everywhere except in the injection plane where a wall boundary condition is applied around the liquid injection. For ELSA calculation, to compute realistically the flow at the exit of the injector, the characteristic size of the mesh cells is about one tenth of the injector diameter. In

21

order to save computational time, the mesh size increases further downstream.

The results presented here have been time-averaged after that the spray tip has left the computational domain. Thus, the Reynolds Averaged Navier Stokes (RANS) results can be compared to the results from DNS calculation. The main variables of the model have been extracted from set of DNS data, in particular: the mean liquid volume fraction $\overline{\phi_l}$ and the mean liquid-gas interface density per unit of volume $\overline{\Sigma} = \overline{\rho}\,\widetilde{\Omega}$.

Fig. 3: (about here)

Planar cuts of the liquid volume fraction field obtained both with the ELSA model and DNS are shown on Fig. 3. The main behaviour of the spray is well captured by the model. It shows the possibility to describe the liquid dispersion induced by complex primary break-up phenomena through a statistical approach and classical turbulent models. To get more quantitative comparisons, profiles have been extracted from the different computational approaches. Location of these profiles can be seen on Fig. 4.

Fig. 4: Position of the different profiles extracted from DNS/ELSA comparisons

First profiles are the reference results from DNS. They are obtained after averaging over 0.1ms since the stabilisation of the injection. The axial profiles (Fig. 5) show that statistical convergence is not perfectly reached yet. Note that the DNS CPU time is roughly 10000 hours on 14 processors (IBM Power 4) and considering running a longer DNS simulation is not realistic. However, the main trend is already well established. Convergence for the mean DNS radial profiles is more satisfactory (see Fig. 6) because they benefit of an additional average by a rotation around the main injection axis. Second profiles concern the result obtained with the ELSA model for the mesh M1 and third profiles are identical but with the refined mesh M2. To

22

get these results, the ELSA model has been implemented in the commercial code FIRE V8.41 (AVL). To evaluate the portability and the sensitivity of the model ELSA, other simulation results are reported here. They have been obtained by the implementation of the model in the commercial code STARCD V3.15 (CD-ADAPCO). Note that it is the same test case but a slightly different mesh is used and an older version of the ELSA model is implemented, in particular the source terms of the surface density equation are different (Beau et al., 2006). Both commercial codes use a finite volume approach and standard equation

Fig. 6 represents the radial profiles of the volume fraction. We observe that even quantitatively good agreements are obtained with respect to the reference data from DNS in all cases. Nevertheless, a closer look to the results shows that $\overline{\phi_l}$ tends to be underestimated by modelling approaches along the injection axis, until the distance from the injector nozzle reaches $8D_{inj}$. These differences are obtained with the two grid refinements. Thus, it probably does not correspond to numerical diffusion. This could be due to the limitations of the gradient law closure to model the turbulent flux of the liquid, (see Eq. (9)). In particular, it is expected that the initial destabilisation of the liquid surface is governed by linear instabilities just at the exit of the injector. Of course, such a turbulent modelling approach used in the ELSA model has to be modified to handle properly these linear instabilities. Some works on that problem have been done elsewhere (Jay et al., 2006) but in a coaxial injector context. Nevertheless, the liquid volume fraction field is accurate enough to allow surface density field to be studied.

Fig. 5: (about here)

Fig. 6: (about here)

The mean surface density field obtained by both DNS and the ELSA model with the mesh M1 are compared on Fig. 7.

23

Fig. 7: (about here)

Since the first proposal (Vallet and Borghi, 1999), the mean surface density equation is still under development. Several models have been proposed for general or specific applications. The surface density equation proposed in Eq. (13) tries to benefit of previous developments with a special attention to the dense zone. The comparisons with the DNS results concerning $\overline{\Sigma}$ are very encouraging. The general shape of the surface density field is well represented. However, a closer look to the data shows a difference on the intensity in the vicinity of the injector. By looking at the DNS picture (Fig. 1) just at the exit of the injector, the liquid surface is perfectly smooth and cylindrical. Thus, the value of $\overline{\Sigma}$ in this case must be zero outside of the surface and infinity at the surface; this is indeed a Dirac function even after averaging. Surface density values extracted from computations are the integral of this surface density in a mesh cell divided by the mesh cell volume. In this area, making the mesh cell bigger in the radial direction does not change the total amount of the surface enclosed in the mesh cell. Consequently, values obtained with the DNS are computed on a finer mesh and then have to be higher than those obtained using the RANS code on a less refined mesh. Another drawback of the comparison concerns the values along the main axis that do not seem similar between ELSA and DNS. To look more precisely at this problem, axial profiles are drawn on Fig. 8.

Fig. 8: (about here)

As far the liquid volume fraction is concerned, the statistical convergence for DNS results is not perfectly reached. Nevertheless, axial profiles of surface density present maxima which are in the same order of magnitude with all the models and in agreement with DNS results. This result has been obtained with the previously given values of the model constants. But it is necessary to keep in mind that, even in DNS, smaller wrinkling than the mesh size are not taken

24

into account by the numerical method. Consequently, the maximum of liquid surface density could be slightly higher. Close to the injector, in the area where the liquid volume fraction estimated with DNS is still equal to unity, there is already a slight decrease of the liquid volume fraction with the ELSA models. That leads to the generation of surface density too early with the models in comparison with the DNS. The distance from the injector where the maximum of surface density is located is not very well established with the DNS due to statistical noise. It can be seen anyway that this distance is under-predicted with both versions of the ELSA model, even if there is an improvement with the present proposal.

Fig. 9: (about here)

Finally, radial profiles of surface density are presented in Fig. 9. ELSA model results compare favourably with the DNS profiles. It seems that the agreement is better a little bit away from the main axis. It also corresponds to a more dilute zone, where the models are more established.

Some conclusions can be drawn from these first validations of the ELSA model in the dense part of the spray obtained thanks to the DNS. First of all, the complex primary break-up phenomena can be handled with the ELSA model even if improvements of the model are still possible. Secondly, for this kind of atomization, the liquid dispersion is well represented by using a turbulent diffusion approach. It is possible to recover a realistic surface density field with the present modelling even in the dense zone of the spray. This is promising to evaluate correctly the surface exchange terms that occur in a spray flame. To go further, the next part deals with macroscopic comparisons with experimental measurements of liquid and vapour penetrations. This study is carried out without changing any modelling constants or numerical parameters in order to test the ability of the ELSA model to predict the spray behaviour and to consider the comparisons with a DNS as a starting point.

4.2 Dilute region of the spray: comparisons between experiments and ELSA calculations

The experimental data have been obtained by classical shadowgraphic technique to get liquid and vapour concentration. Two different injectors are tested for two injection pressures (see the figure 10 for the velocity profiles). The two injectors have the same diameter $D_{inj} = 148\,\mu m$. Two different gas chamber temperatures are tested: $T_{ch} = 790 - 935°K$. In all the studied cases, the back-pressure (chamber pressure) is kept constant and equal to 7MPa. All experimental conditions are summarized in table 2. These data are typical Diesel-like conditions encountered in present engines.

Table 2: (about here)

The computational domain corresponds to a cylinder of a diameter of 5mm and a high of 23.5mm. Wall boundary conditions are applied everywhere except at the liquid inlet where a mass flow rate is imposed. The amount of cell divisions along the injector diameter is about 10. The number of cells for the total computational grid used for these calculations is 90000. Concerning the liquid turbulence that is initialized at the nozzle exit, an intensity of 5% of the bulk velocity has been retained and a turbulent length scale of 10% of the injector diameter has been chosen.

To compute the vapour penetration, it is necessary to introduce a rate of mass and heat transfer across the interface. Additionally, it is expected that a unique temperature for the mixture, the liquid and the gas is not adapted to this kind of injection process. In the following, results have been obtained by introducing an equation for the mean mixture enthalpy $\overline{\rho}\,\widetilde{h}_{mix}$ and for the mean liquid enthalpy $\overline{\rho}\,\widetilde{Y}_l\,\widetilde{h}_l$. From these equations the mean liquid temperature $\widetilde{T}_l$ is recovered from the following relation:

$$\widetilde{h}_l = \int_{T^0}^{\widetilde{T}_l} Cp\, dT \tag{32}$$

and the mean gas temperature thanks to the relation:

$$\int_{T^0}^{\widetilde{T}_g} Cp_g\, dT = \frac{\widetilde{h}_{mix} - \widetilde{Y}_l \widetilde{h}_l}{1 - \widetilde{Y}_l}. \tag{33}$$

Heat and mass transfer have to be described through the liquid–gas interface but it remains a very difficult problem in the dense part of the spray. Available models are mainly based on the exchange between a spherical droplet and an ambient gas. As a first approach, this kind of model is applied here. We first determine a droplet diameter at every location where there is a non negligible amount of liquid thanks to the Eq. (19). The amount Q of heat transfer to one droplet and the amount of mass transfer $\dot{m}_{vap}$ due to the vaporization of one droplet are determined classically (Abramzon and Sirignano, 1989). The temperature of the droplet is taken as $\widetilde{T}_l$, the temperature of the gas as $\widetilde{T}_g$ and the slipping velocity between the gas and the droplet as Δv_{rel}. By dividing Q and $\dot{m}_{vap}$ by the surface of one droplet πD^2, the estimation of the rate of heat and mass transfer per unit of surface is obtained. The total mass of heat transfer per unit of volume is obtained by multiplying the rate for one droplet by the total surface per unit of volume $\overline{\rho}\,\widetilde{\Omega}$. Finally, the remaining source terms are for the mean liquid enthalpy $\overline{\rho}\,\widetilde{Y}_l\,\widetilde{h}_l$:

$$\overline{\rho}\,\widetilde{\Omega}\frac{\left(Q - \dot{m}_{vap}\right)}{\pi D^2} \tag{34}$$

and for the mean mixture enthalpy $\overline{\rho}\,\widetilde{h}_{mix}$:

$$\overline{\rho}\,\widetilde{\Omega}\frac{\dot{m}_{vap} L_v}{\pi D^2}, \tag{35}$$

where L_v is the latent heat of vaporization.

It can be considered as a draw back of the present model to use a dilute approximation in the dense zone of the spray for vaporisation although a special effort has been done up to now to avoid this strong simplification. At least for Diesel applications in the dense part of the spray, the

27

amount of energy and of vapour that can be incorporated in the gas is very small by comparison to the liquid part. Accordingly, the saturation is reached very quickly. In our experience, this can even create numerical instabilities. Hence special care is devoted to compute the saturation state (final concentration of liquid, vapour and final temperature) everywhere in the spray and at each time step. The delay which is necessary to reach this state is driven by the vaporization in this zone. Since the saturation state is obtained almost instantaneously, the model for vaporization in this zone is not so important.

Concerning the effect of the vaporization on the surface density equation, a simple model that represents the decrease of surface that is linked to the decrease of the droplet radius is retained:

$$S_{vapo} = -\frac{2\overline{\rho}\,\tilde{\Omega}^2}{3\tilde{Y}_l}\frac{\dot{m}_{vap}}{\pi D^2}.$$ (36)

Because this model corresponds to the reduction of surface in a spray of droplets, it should not be valid in the dense zone of the spray. Indeed, it is not sure that the vaporization term decreases the surface density. It should depend if the considered surface is concave or convex. For instance, if the two phase flow contains bubbles, vaporization should increase the surface area. Anyway, the additional velocity of the interface due to the vaporization is usually negligible in comparison with the velocity induced by turbulence motion.

Comparisons of experimental data and results obtained with the ELSA model for conditions given in Table 2 are presented on Fig. 11-14.

Fig. 11 : (about here)

Fig. 12 : (about here)

Fig. 13 : (about here)

Fig. 14 : (about here)

In all studied cases, liquid and vapour penetrations calculated by the ELSA model are in good agreements with measurements. With a higher injection pressure, the vapour penetrations are

28

growing faster, whereas the liquid penetrations are less affected (see Fig. 11-14 for comparisons). This phenomenon also appears when switching from the injector 1 to the injector 2 at P_{inj}=54MPa: the velocity profile for injector 2 grows faster than for injector 1. Thus, the vapour penetrations are growing faster with the injector 2 than with the injector 1. Simultaneously, the liquid penetration does not change a lot. These behaviours are directly linked to the temporal evolution of the velocity at the exit of the injector, (Fig. 10). The vapour penetration is directly linked to the mass flow rate of the injector but the liquid penetration is the result of two conflicting phenomena: the increase of velocity makes the liquid penetration growing faster and the turbulence mixing increases the vaporisation rate which reduces the liquid penetration. The differences between the two injectors are less significant with an injection pressure P_{inj}=180MPa. This is in agreement with the injection velocities which are less different at high injection pressure. All these phenomena are observed experimentally and recovered by the numerical model.

These liquid and vapour penetrations are classically shown when testing an atomization model, and they confirm that the ELSA model behave at least as good as the other models. Note that constants and parameters of the model were fixed thanks to the DNS and nothing like "user parameters" are used to fit the model. However, it is possible that the details of the primary break-up model are not of primary importance to recover the effects of velocity injection, back-pressure or nozzle diameter changes. These last two evaluations were also performed successfully with the ELSA model (Lebas et al., 2005). But accordingly to Yi and Reitz (Yi and Reitz, 2004) and to our experience, the effect of gas temperature changes can be captured accurately only if special care is dedicated to the primary break-up that occurs in the dense zone of the spray. In Fig. 11-14, the vapour penetrations are not very affected by the change of gas temperature whereas the liquid penetrations decrease from about 15mm to 12mm. This is observed experimentally for the two kinds of injector and for the two injection pressures. The shorter liquid penetration due to the increase of the gas temperature is the result of a competition

between the mass flow rate, the turbulent mixing and the vaporization. The ELSA model is able to recover the decrease of the liquid penetration, still keeping the vapour penetration unchanged. This is a possible benefit of a better representation of the vaporisation thanks to the surface density equation.

Fig. 15: (about here)

The Fig. 15 presents a spatial distribution of the equivalence ratio at an injection pressure of 180MPa for injector 2 and two different gas chamber temperatures 790°K and 935°K. It can be observed that there is no vaporized fuel near the injector nozzle. It is mainly due to the fact that the density of the spray prevents the liquid from being heated by the surrounding gas and vaporized. In fact, in this region of the spray, a saturated state of vaporization is quickly reached, considering the small values of air mass fraction. It is a key point of the ELSA model because this dense region of the spray cannot be represented by a Lagrangian approach which considers the liquid volume as negligible. Moreover, it is interesting to notice that despite a similar vapour penetration (that does not change with the temperature) the equivalence ratio field is very different for the two considered gas temperatures. This is of primary importance for the combustion.

To build a complete modelling approach which is able to represent the two phase flow combustion, the model of combustion ECFM-3Z (Colin and Benkenida, 2004) has been coupled to the atomization model ELSA. The test case corresponds to an experiment of Diesel flame (Higgins and Siebers, 2001). It consists in an injector of 180μm diameter hole, with an injection pressure of 138MPa. The OH self emission of the flame is recorded to measure the position of the flame lift-off. Two gas temperatures are considered, 1000°K and 1200°K. Results are presented on Fig. 16.

Fig. 16: (about here)

White lines show the measured flame lift-off mean position. Close to the injector exit, the red zone represents the surface where the liquid mass fraction is upper than 0.01 ($\tilde{Y}_l > 0.01$). Flames obtained with numerical simulations seem to expand a little more in the radial direction than experimental flames. Additionally the flame lift-off is a little bit overestimated for the gas temperature of 1000°K. Nevertheless, as expected when looking at the equivalence ration field (Fig. 15), the gas temperature also influences the shape of the flame. It is found in the experiment that increasing the gas temperature makes the flame lift-off distance decreasing. This is due to a stronger vaporization which reduced the distance to achieve a stochiometric mixture, which is necessary to stabilize the flame. This behaviour is well captured by the model. Additionally, the radial expansion of the flame is reduced by increasing the gas temperature. This trend is also observed numerically.

5 Conclusion

This work presents recent developments in the modelling of the atomization of sprays, in particular in the description of the primary break-up. The dense zone of the spray is difficult to characterize experimentally. Thanks to progress in direct numerical simulation of two phase flows based on LS/VOF/GF (Menard et al., 2007), quantitative results have been obtained for the first time where experiments failed to provide data in Diesel spray. These results have been used to develop and to assess a model devoted to the dense zone of the atomization, the so-called ELSA model. This model was originally proposed by Vallet and Borghi (Vallet and Borghi, 1999) and the presented version incorporates recent developments in particular for the dense part of the spray. With this version, the modelling proposal has been applied successfully in the dense zone of the spray when comparing to the DNS data. Modelling parameters and constants have

31

been fixed by comparisons with DNS data. Without changing these parameters, a vaporization model has been joined to the atomization model and the entire approach has been tested successfully on experimental data in terms of liquid and vapour penetrations. In particular, the ELSA model has been able to recover the influence of gas temperature changes. Experiments show that the liquid penetration decreases when the gas temperature increases but the vapour penetrations have been found unchanged. This trend is well recovered by the model but the presented results show that for different gas temperatures, similar vapour penetrations lead to different equivalence ratio fields. This must be important for combustion, accordingly a combustion model ECFM-3Z has been coupled to the ELSA approach to model an experiment of Diesel flame lift-off. The influence of initial gas temperature on the flame lift-off found experimentally has been well represented by the complete modelling proposal.

6 Acknowledgments

7 References

Abramzon, B. and Sirignano, W. A., 1989. Droplet vaporization model for spray combustion calculations. International Journal of Heat and Mass Transfer, 32 (9), 1605-1618.

AVL, User guide for FIRE. www.avl.com,

Beale, J. C. and Reitz, R. D., 1999. Modeling spray atomization with the Kelvin-Helmholtz/Rayleigh-Taylor hybrid model. Atomization and Sprays: Journal of the International Institutions for Liquid Atomization and Spray Systems, 9 (6), 623-650.

Beau, P. A., Funk, M., Lebas, R. and Demoulin, F. X., 2005. Applying quasi-multiphase model to simulate atomization processes in Diesel engines: Modeling of the slip velocity. SAE Technical Papers, 2005-01-0220

Beau, P. A., Menard, T., Lebas, R., Berlemont, A., Tanguy, S. and Demoulin, F. X., 2006. Numerical jet atomization. Part II: modeling information and comparison with DNS results. Miami, FL, United States, American Society of Mechanical Engineers, New York, NY 10016-5990, United States.

Beheshti, N., Burluka, A. A. and Fairweather, M., 2007. Assessment of summation -Y liq model predictions for air-assisted atomisation. Theoretical and Computational Fluid Dynamics, 21 (5), 381-397.

Blaisot, J. B. and Yon, J., 2005. Droplet size and morphology characterization for dense sprays by image processing: application to the Diesel spray. Experiments in Fluids, V39 (6), 977-994.

Blokkeel, G., Borghi, R. and Barbeau, B., 2003. A 3d Eulerian model to improve the primary breakup of atomizing jet. SAE Technical Papers, 2003-01-0005

Cai, W., Powell, C. F., Yue, Y., Narayanan, S., Wang, J., Tate, M. W., Renzi, M. J., Ercan, A., Fontes, E. and Gruner, S. M., 2003. Quantitative analysis of highly transient fuel sprays by time-resolved x-radiography. Applied Physics Letters, 83 (8), 1671-1673.

CD-ADAPCO, User manuel for STAR-CD. www.cd-adapco.com,

Chaves, H., Kirmse, C. and Obermeier, F., 2004. Velocity measurements of dense diesel fuel sprays in dense air. Atomization and Sprays, 14 (6), 589-609.

Colin and Benkenida, A., 2004. The 3-zones extended coherent flame model (ecfm-3z) for computing prmixed/diffusion combustion. Oil and Gas Science and Technology, 59(6) 593-609.

Demoulin, F.-X., Beau, P.-A., Blokkeel, G., Mura, A. and Borghi, R., 2007. A new model for turbulent flows with large density fluctuations: Application to liquid atomization. Atomization and Sprays, 17 (4), 315-345.

Enright, D., Fedkiw, R., Ferziger, J. and Mitchell, I., 2002. A Hybrid Particle Level Set Method for Improved Interface Capturing. Journal of Computational Physics, 183 (1), 83-116.

Fedkiw, R. P., Aslam, T., Merriman, B. and Osher, S., 1999. A Non-oscillatory Eulerian Approach to Interfaces in Multimaterial Flows (the Ghost Fluid Method). Journal of Computational Physics, 152 (2), 457-492.

Higgins, B. S. and Siebers, D. L., 2001. Measurement of the flame lift-off location on Diesel Sprays using OH chemiluminescence. SAE Technical Papers, 2001010918

Ishii, M., 1975. Thermo-fluid dynamic theory of two-phase flow. Paris, Eyrolles.

Ishii, M., 1977. One-dimensional Drift-flux model and constitutive equations for relative motion between phases in various two-phase flow regimes. Argonne National Lab., (ANL-77-47),

Ishii, M. and Ibiki, T., 2006. Thermo-Fluid Dynamics Of Two-phase Flow. New York, Springer.

Iyer, V. and Abraham, J., 2003. An evaluation of a two-fluid Eulerian-liquid Eulerian-gas model for diesel sprays. Journal of Fluids Engineering, Transactions of the ASME, 125 (4), 660-669.

Iyer, V. A., Abraham, J. and Magi, V., 2002. Exploring injected droplet size effects on steady liquid penetration in a Diesel spray with a two-fluid model. International Journal of Heat and Mass Transfer, 45 (3), 519-531.

Jay, S., Lacas, F. and Candel, S., 2006. Combined surface density concepts for dense spray combustion. Combustion and Flame, 144 (3), 558-577.

Kang, M., Fedkiw, R. P. and Liu, X. D., 2000. A boundary condition capturing method for multiphase incompressible flow. Journal of Scientific Computing, 15 (3), 323-360.

Kataoka, I., 1986. Local instant formulation of two-phase International Journal of Multiphase Flow, 12 (5), 745-758.

Kocamustafaogullari, G. and Ishii, M., 1995. Foundation of the interfacial area transport equation and its closure relations. International Journal of Heat and Mass Transfer, 38 (3), 481-493.

Launder, B. E. and Spalding, D. B., 1974. NUMERICAL COMPUTATION OF TURBULENT FLOWS. Computer Methods in Applied Mechanics and Engineering, 3 (2), 269-289.

Lebas, R., Blokkeel, G., Beau, P. A. and Demoulin, F. X., 2005. Coupling vaporization model with the Eulerian-Lagrangian Spray Atomization (ELSA) model in Diesel engine conditions. SAE Technical Papers, 2005-01-0213

Linne, M., Paciaroni, M., Hall, T. and Parker, T., 2006. Ballistic imaging of the near field in a diesel spray. Experiments in Fluids, 40 (6), 836-846.

Liu, X.-D., Fedkiw, R. P. and Kang, M., 2000. A Boundary Condition Capturing Method for Poisson's Equation on Irregular Domains. Journal of Computational Physics, 160 (1), 151-178.

Marble, F. E. and Broadwell, J. E., 1977. The coherent flame model for turbulent chemical reactions. Purdue University, West Lafayette, IN,

Marmottant, P. H. and Villermaux, E., 2004. On spray formation. Journal of Fluid Mechanics, 498 (498), 73-111.

Menard, T., Tanguy, S. and Berlemont, A., 2007. Coupling level set/VOF/ghost fluid methods: Validation and application to 3D simulation of the primary break-up of a liquid jet. International Journal of Multiphase Flow, 33 (5), 510-524.

Morel, C., 2007. On the surface equations in two-phase flows and reacting single-phase flows. International Journal of Multiphase Flow, 33 (10), 1045-1073.

Olsson, E. and Kreiss, G., 2005. A conservative level set method for two phase flow. Journal of Computational Physics, 210 (1), 225-246.

Osher, S. and Fedkiw, R. P., 2001. Level Set Methods: An Overview and Some Recent Results. Journal of Computational Physics, 169 (2), 463-502.

Park, H., Yoon, S. S. and Heister, S. D., 2005. A nonlinear atomization model for computation of drop size distributions and spray simulations. International Journal for Numerical Methods in Fluids, 48 (11), 1219-1240.

Pilch, M. and Erdman, C. A., 1987. Use of breakup time data and velocity history data to predict the maximum size of stable fragments for acceleration-induced breakup of a liquid drop. International Journal of Multiphase Flow, 13 (6), 741-757.

Plateau, J., 1873. Statique Expérimentale et Théorique des Liquides Soumis aux Seules Forces Moléculaires. Gautier-Villars. Paris,

Ponstein, J., 1959. Instability of rotating cylindrical jets. Appl. Sci. Res. , A8

Qian, J. and Law, C. K., 1997. Regimes of coalescence and separation in droplet collision. Journal of Fluid Mechanics, 331 59-80.

Rayleigh, L., 1878. On The Instability Of Jets. Proc. London Math. Soc., s1-10 (1), 4-13.

Reitz, R. D., 1987. Modeling Atomization Processes in High-Pressure Vaporizing Sprays. Atomisation and Spray Technology, 3 309-337.

Sethian, J. A., 1996. A fast marching level set method for monotonically advancing fronts. Proceedings of the National Academy of Sciences of the United States of America, 93 (4), 1591.

Sidhu, M. S. and Burluka, A. A., 2008. Average vaporisation rate in turbulent subcritical two-phase flow. Combustion Science and Technology, 180 (5), 975-996.

Simonin, O., 2000. Statistical and continuum modelling of turbulent reactive particulate flows. Lecture Series 1996-02, Von Karman Institute for Fluid Dynamics,

Sussman, M., Fatemi, E., Smereka, P. and Osher, S., 1998. Improved level set method for incompressible two-phase flows. Computers & Fluids, 27 (5-6), 663-680.

Sussman, M. and Puckett, E. G., 2000. A Coupled Level Set and Volume-of-Fluid Method for Computing 3D and Axisymmetric Incompressible Two-Phase Flows. Journal of Computational Physics, 162 (2), 301-337.

Vallet, A. and Borghi, R., 1999. Modélisation Eulerienne de L'atomisation d'un Jet Liquide. C. R. Acad. Sci., Paris, Sér. II b, 327 1015–1020.

Vallet, A., Burluka, A. A. and Borghi, R., 2001. Development of a Eulerian model for the "Atomization" of a liquid jet. Atomization and Sprays, 11 (6), 619-642.

van der Pijl, S. P., Segal, A., Vuik, C. and Wesseling, P., 2005. A mass-conserving Level-Set method for modelling of multi-phase flows. International Journal for Numerical Methods in Fluids, 47 (4), 339-361.

Villermaux, E., 2007. Fragmentation. Annual Review of Fluid Mechanics, 39 419-446.

Yi, Y. and Reitz, R. D., 2002. A one-dimensional breakup model for low-speed jets. Automization and Sprays: Journal of the International Institutions for Liquid Atomization and Spray Systems, 12 (5-6), 667-685.

Yi, Y. and Reitz, R. D., 2004. Modeling the primary breakup of high-speed jets. Atomization and Sprays, 14 (1), 53-80.

Yoon, S. S., 2005. Droplet distributions at the liquid core of a turbulent spray. Physics of Fluids, 17 (3), 035103-1.

Yoon, S. S. and Heister, S. D., 2004. A fully non-linear model for atomization of high-speed jets. Engineering Analysis with Boundary Elements, 28 (4), 345-357.

Yue, Y., Powell, C. F., Poola, R., Wang, J. and Schaller, J. K., 2001. Quantitative measurements of diesel fuel spray characteristics in the near-nozzle region using X-ray absorption. Atomization and Sprays, 11 (4), 471-490.
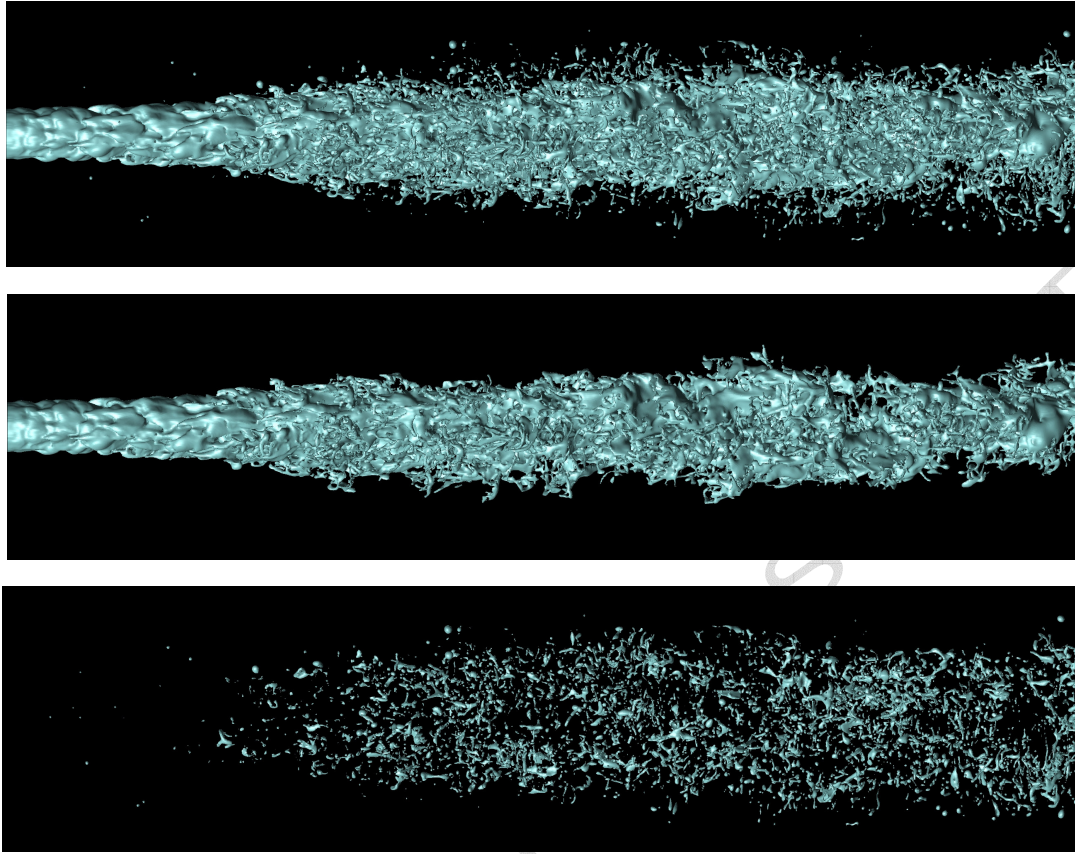
Fig. 1: Visualization of a spray obtained from DNS computation. From top to bottom: Complete spray; Liquid part attached to the injector tip; detached part of the liquid
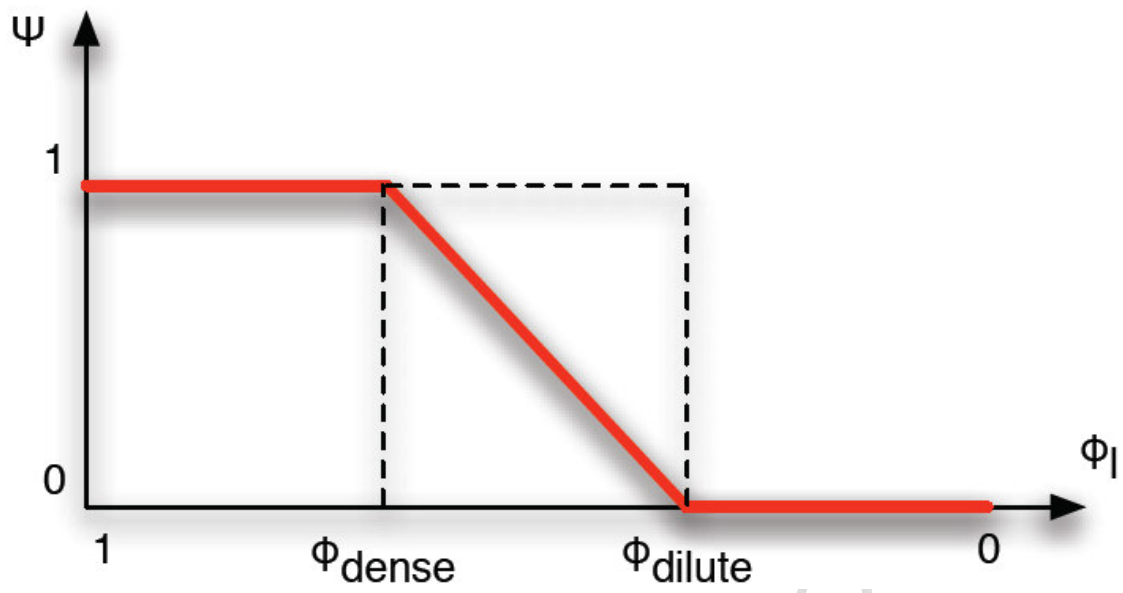
Fig. 2: Indicator function Ψ used to share out dense and dilute source terms used in the surface density equation.
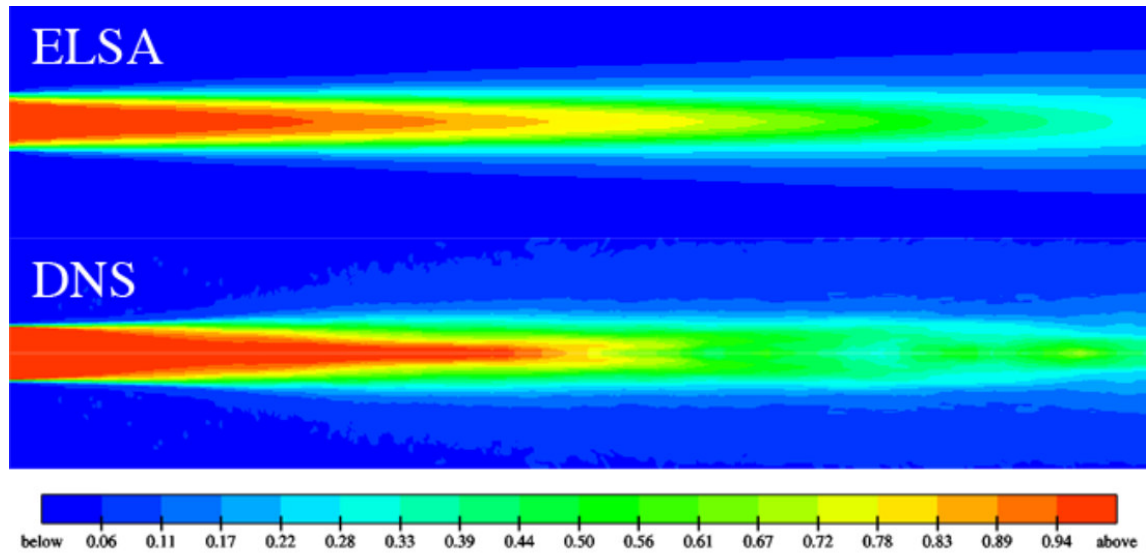
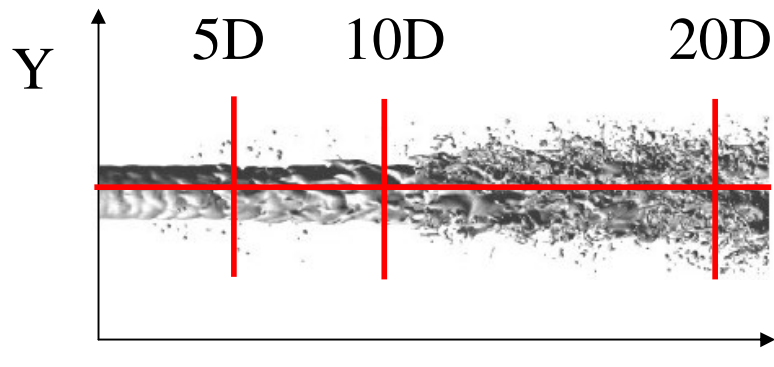Fig. 3: Cut of the liquid volume fraction field obtained by using the ELSA model (top) and DNS (bottom)

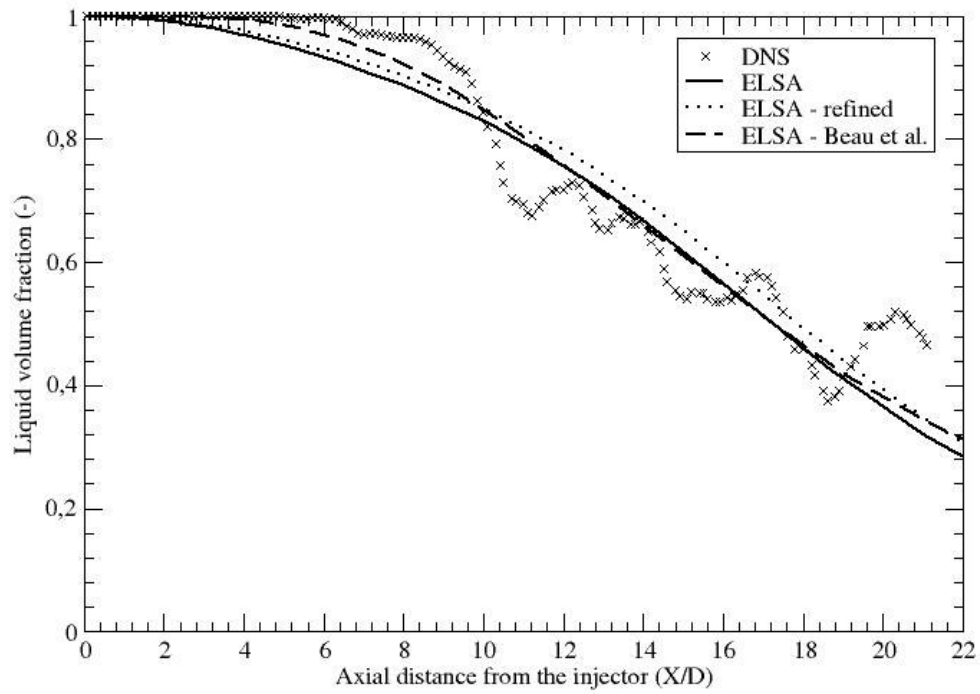Fig. 4: Position of the different profiles extracted from DNS/ELSA comparisons

Fig. 5:   Axial profile of the liquid volume fraction $\overline{\phi}_l$. Symbols is DNS (), solid line is ELSA model with standard mesh, dotted line is ELSA model with refined mesh   and dashed line is ELSA model by   (Beau et al., 2006)

39

Liquid volume fraction (-)
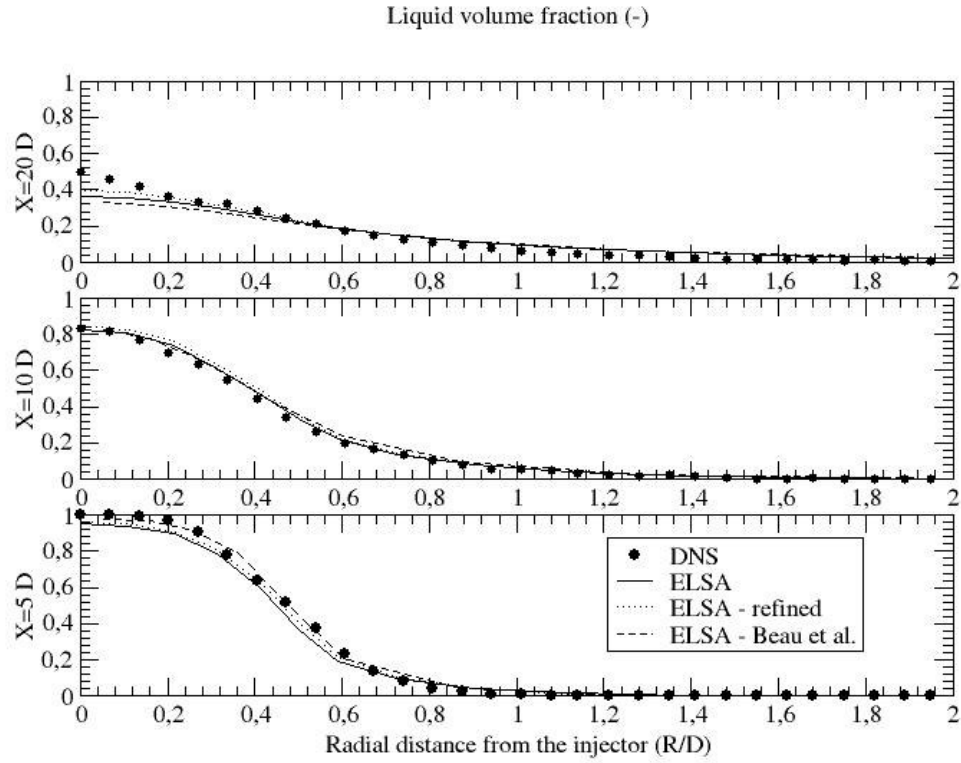
Fig. 6:   Radial profiles of the liquid volume fraction $\overline{\phi_l}$ from bottom to the top at 5, 10 and
20 diameter from the injector. Legend is identical to Fig. 6.
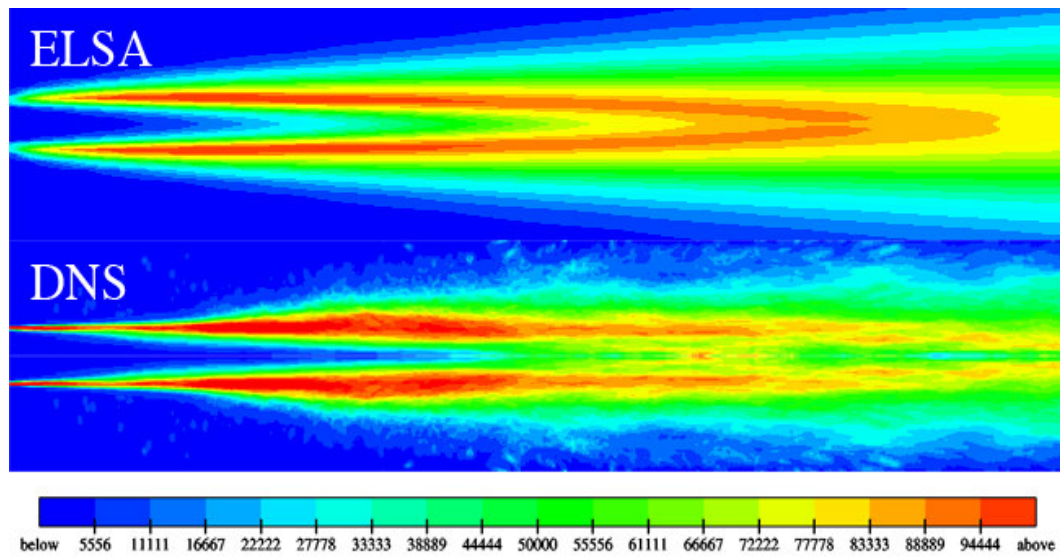
Fig. 7: Cut of the liquid-gas surface density $\overline{\Sigma}$ field obtained by using the ELSA model (top) and DNS (bottom)
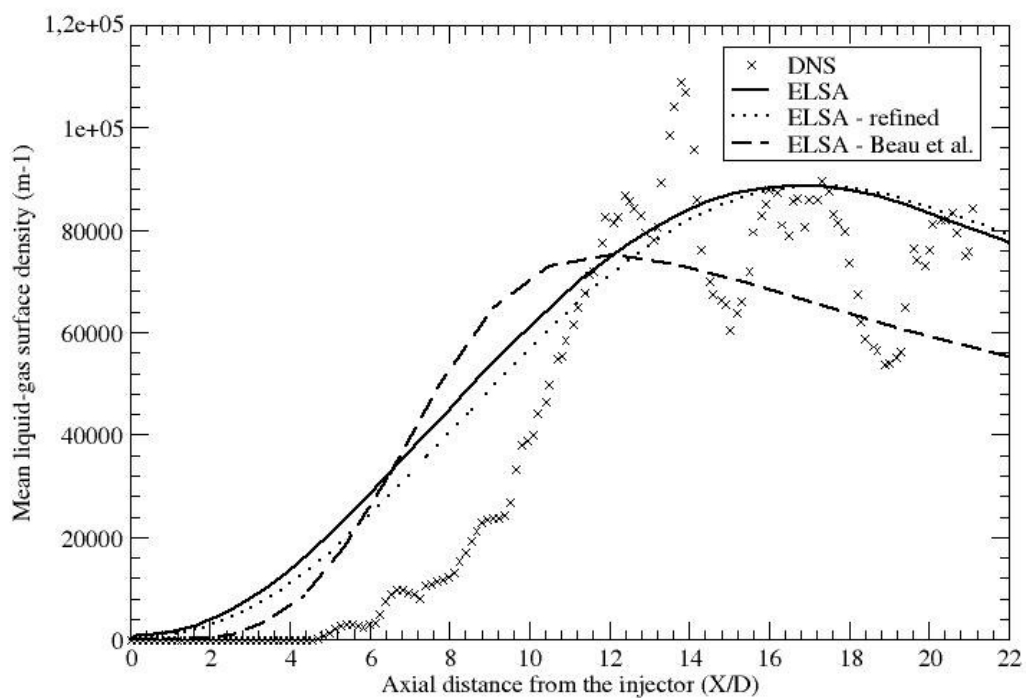
Fig. 8:   Axial profiles of the liquid-gas surface density $\overline{\Sigma}$. Legend is identical to Fig. 6.

Meand liquid-gas surface density (m-1)
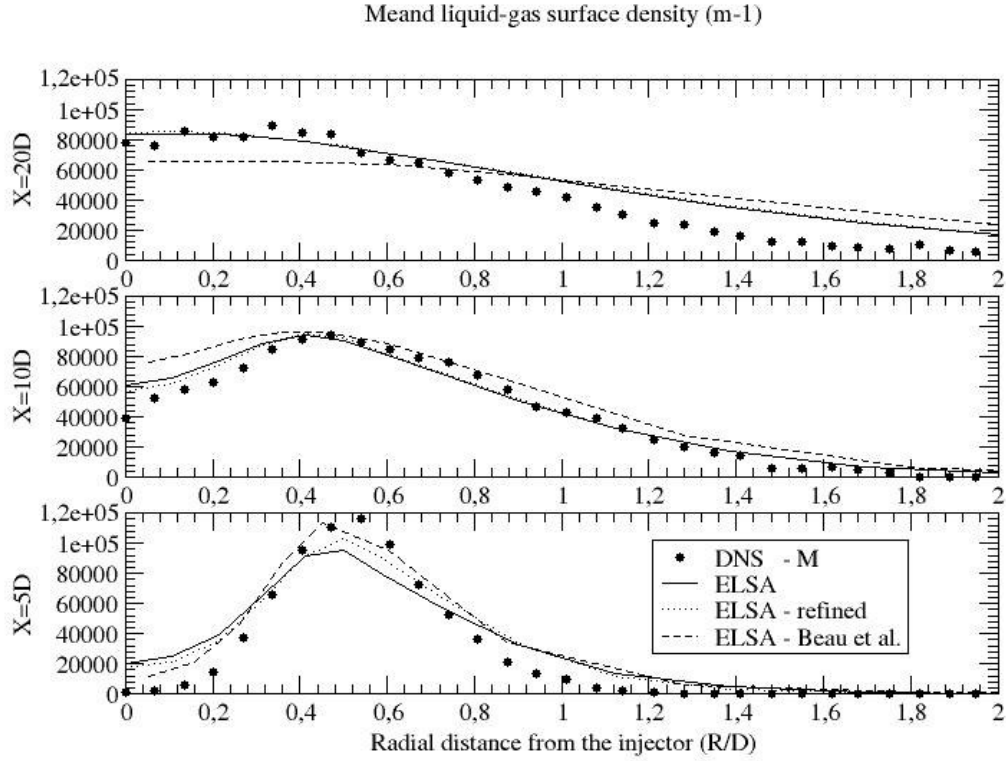
Fig. 9: Radial profiles of the liquid-gas surface density $\overline{\Sigma}$, from bottom to the top at 5, 10 and 20 diameters from the injector. Legend is identical to Fig. 6.
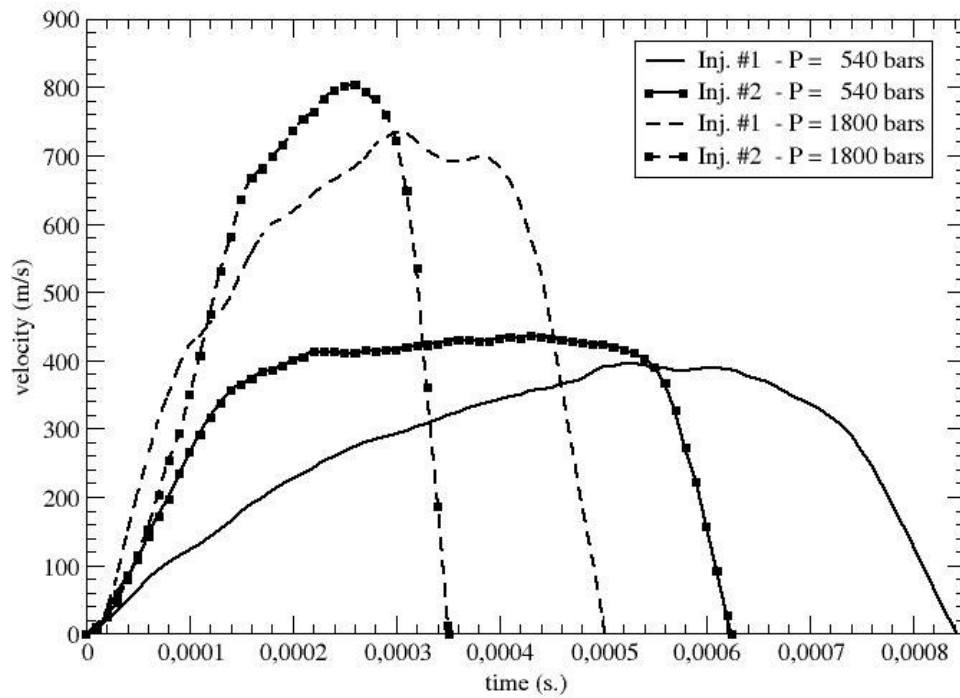
Fig. 10: Temporal evolution of the velocity at the exit of the injector depending on the injector type and on the injection pressure
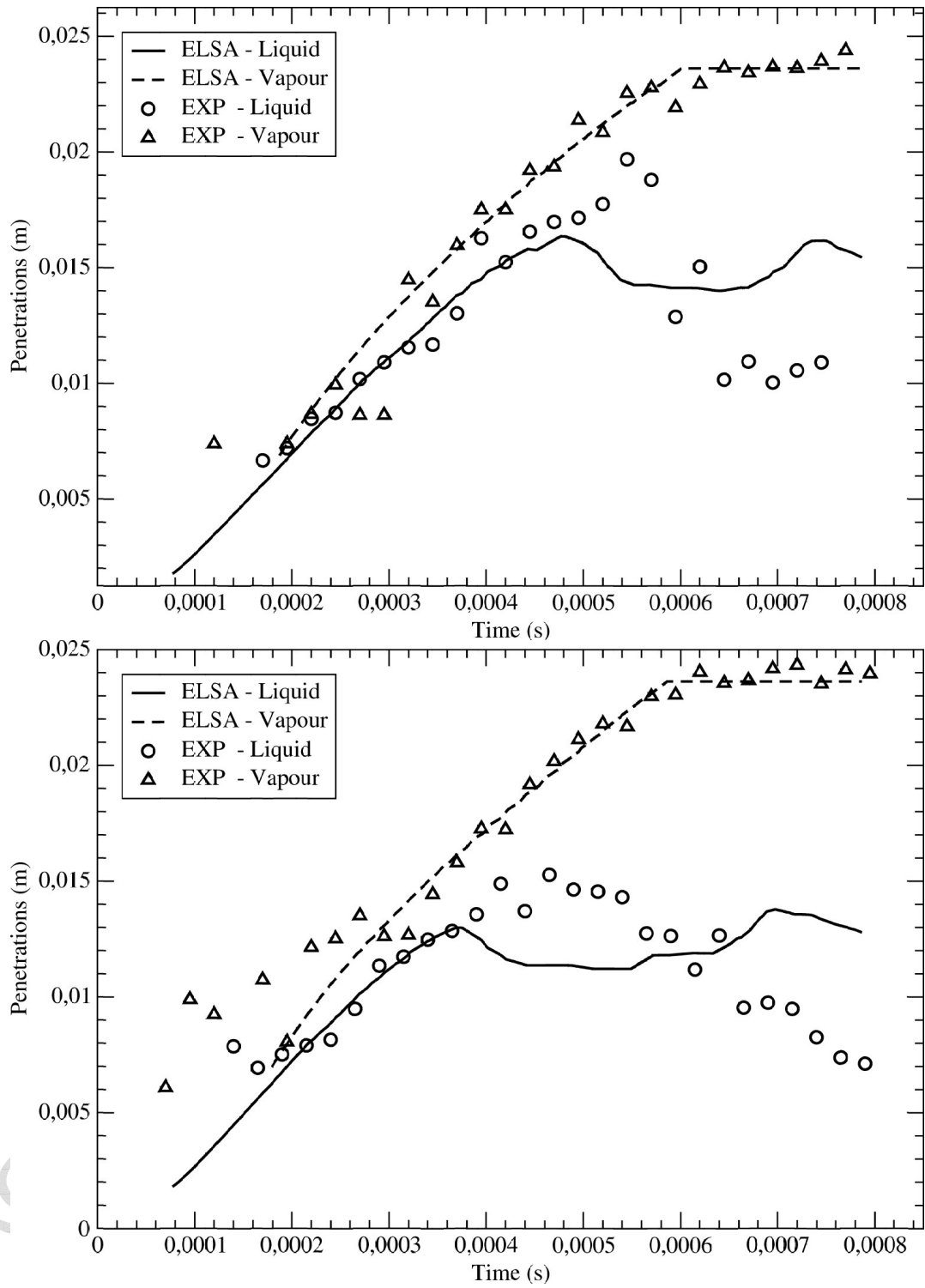
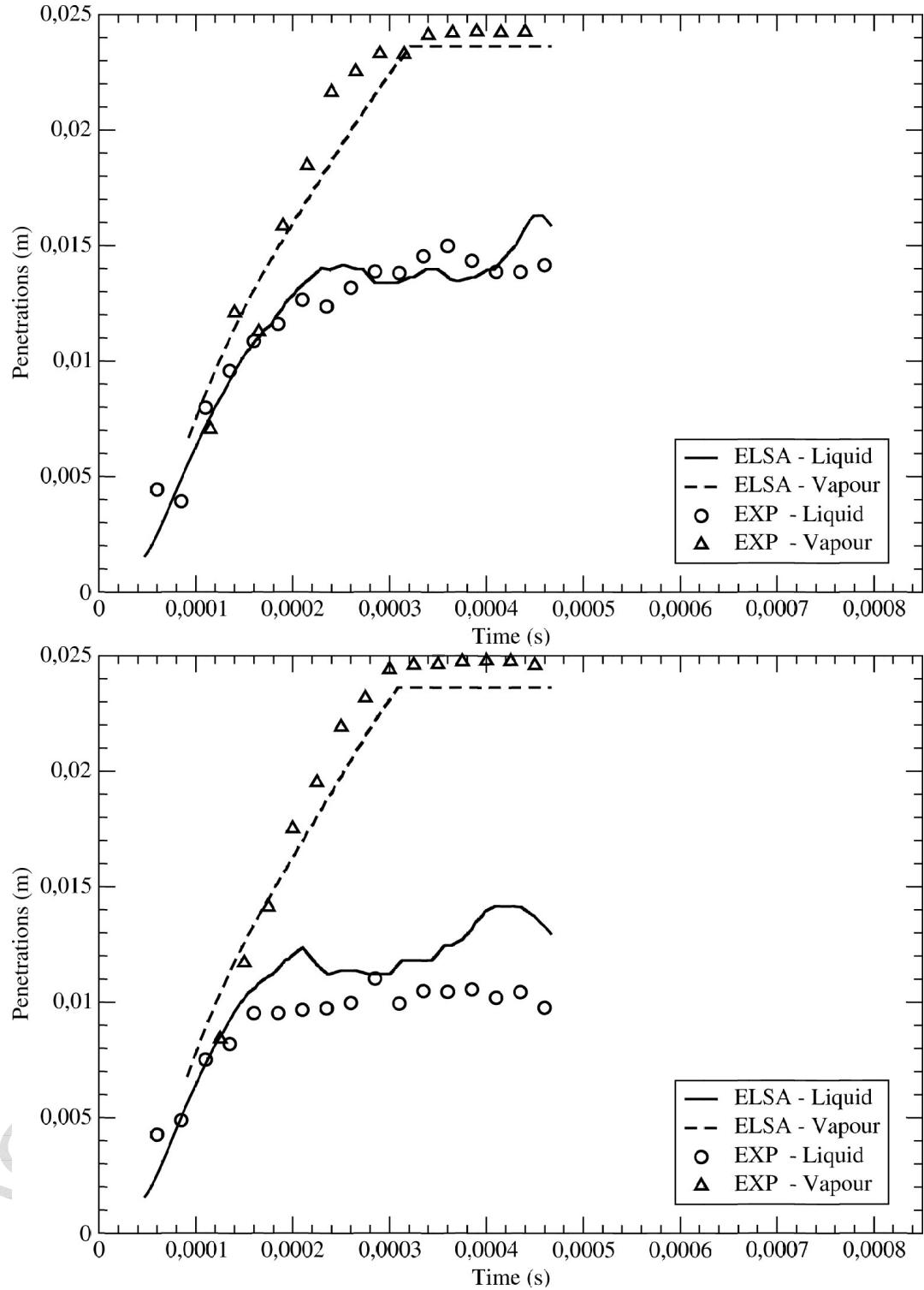Fig. 11: Liquid and vapour penetration for the injector 1 for $P_{inj} = 54MPa$: Top $T_{ch} = 790°K$; Bottom $T_{ch} = 935°K$
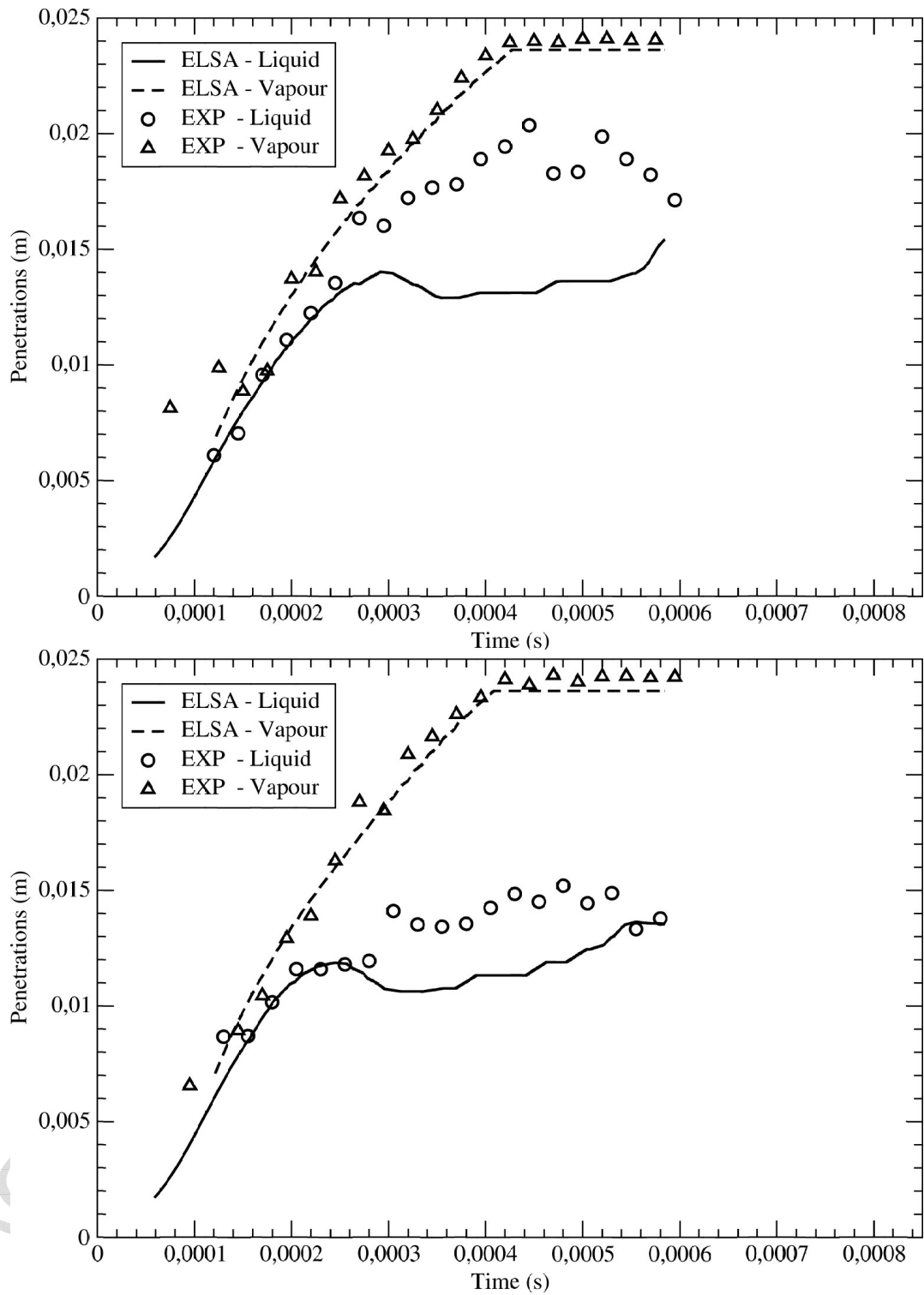
Fig. 12: Liquid and vapour penetration for the injector 2 for $P_{inj} = 54MPa$: Top $T_{ch} = 790°K$;
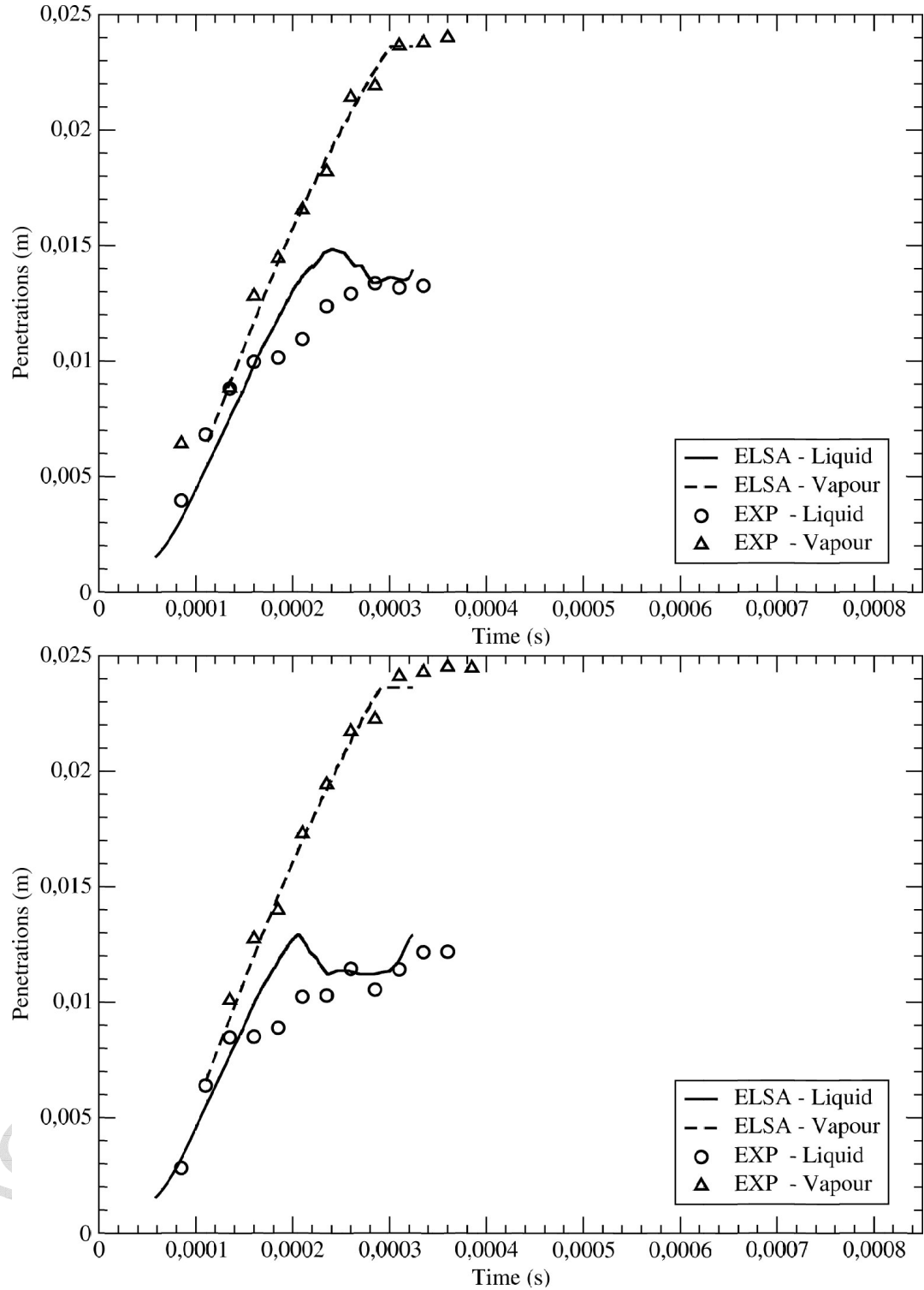
Bottom $T_{ch} = 935°K$

Fig. 13: Liquid and vapour penetration for the injector 1 for $P_{inj} = 180MPa$: Top $T_{ch} = 790°K$;
Bottom $T_{ch} = 935°K$

Fig. 14: Liquid and vapour penetration for the injector 2 for $P_{inj} = 180MPa$: Top $T_{ch} = 790°K$;
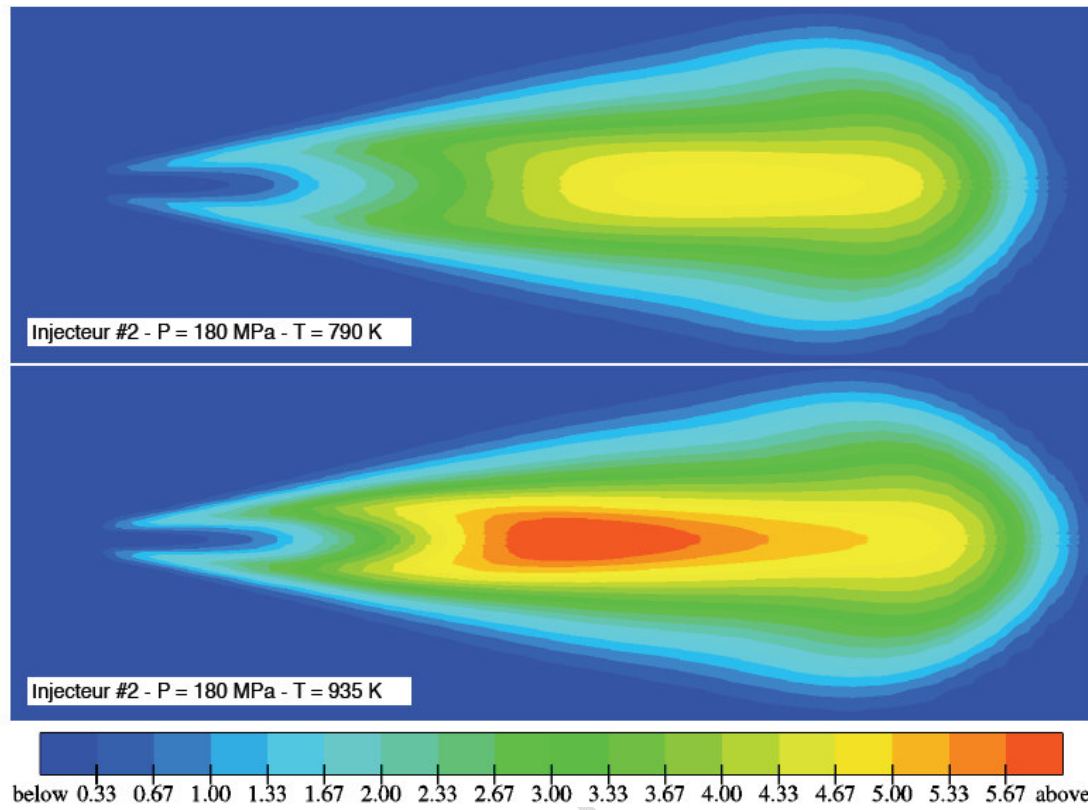
Bottom $T_{ch} = 935°K$

Fig. 15: Equivalence ration field for injector 2, P_{inj}=180MPa, 0.3 ms after the start of injection. Top $T_{ch} = 790°K$ and bottom $T_{ch} = 935°K$
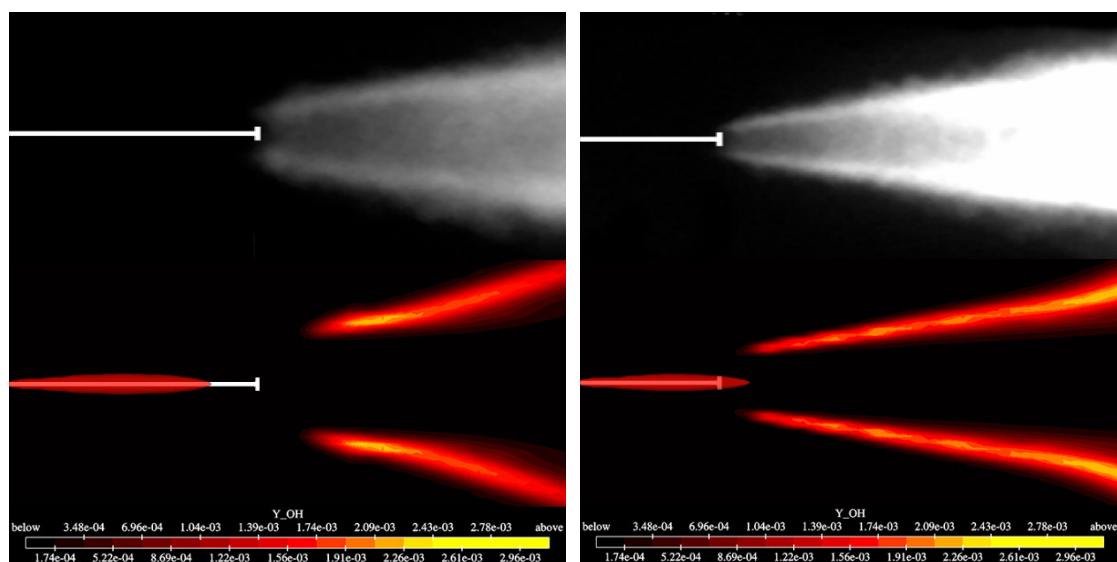
Fig. 16: Comparison of OH self emission obtained experimentally (top) to OH concentration computed using the model ELSA combined to the model ECFM-3Z (bottom) for two gas temperatures $T_{ch} = 1000°K$ (left) and $T_{ch} = 1200°K$ (right).

50

Liquid Injection	Turbulent Intensity	Turbulent Length Scale	Velocity	Injector Diameter	
	5%	$10\mu m$	$100 m.s.^{-1}$	$100\mu m$	
Property	Surface tension	Liquid Density	Gas Density	Liquid viscosity	
	$0.06 kg.s.^{-2}$	$696 kg.m.^{-3}$	$50 kg.m.^{-3}$	1.2×10^{-3} kg.m^{-1}.s^{-1}	

Table1: Presentation of the test case studied by DNS.

Injection pressure	54MPa	180MPa
Injector N°	1	2
Chamber temperature	780°K	935°K
Density	30kgm^{-3}	25kgm^{-3}

Table 2: Experimental conditions for liquid and vapour concentration